Automated isotopic measurements of micron-sized dust: Application to meteoritic presolar silicon carbide

LARRY R. NITTLER* and CONEL M. O'D. ALEXANDER

Department of Terrestrial Magnetism, Carnegie Institution of Washington, 5241 Broad Branch Road NW, Washington, D.C. 20015, USA

Abstract—We report the development of a new analytical system allowing the fully automated measurement of isotopic ratios in micrometer-sized particles by secondary ion mass spectrometry (SIMS) in a Cameca ims-6f ion microprobe. Scanning ion images and image processing algorithms are used to locate individual particles dispersed on sample substrates. The primary ion beam is electrostatically deflected to and focused onto each particle in turn, followed by a peak-jumping isotopic measurement. Automatic measurements of terrestrial standards indicate similar analytical uncertainties to traditional manual particle analyses (e.g., ~3‰/amu for Si isotopic ratios). We also present an initial application of the measurement system to obtain Si and C isotopic ratios for ~3300 presolar SiC grains from the Murchison CM2 carbonaceous chondrite. Three rare presolar Si_3N_4 grains were also identified and analyzed. Most of the analyzed grains were extracted from the host meteorite using a new chemical dissolution procedure. The isotopic data are broadly consistent with previous observations of presolar SiC in the same size range (~0.5–4 μm). Members of the previously identified SiC AB, X, Y, and Z subgroups were identified, as was a highly unusual grain with an extreme ^{30}Si enrichment, a modest ^{29}Si enrichment, and isotopically light C. The stellar source responsible for this grain is likely to have been a supernova. Minor differences in isotopic distributions between the present work and prior data can be partially explained by terrestrial contamination and grain aggregation on sample mounts, though some of the differences are probably intrinsic to the samples. We use the large new SiC database to explore the relationships between three previously identified isotopic subgroups—mainstream, Y, and Z grains—all believed to originate in asymptotic giant branch stars. The isotopic data for Z grains suggest that their parent stars experienced strong CNO-cycle nucleosynthesis during the early asymptotic giant branch phase, consistent with either cool bottom processing in low-mass (M < $2.3M_\odot$) parent stars or hot-bottom burning in intermediate-mass stars (M > $4M_\odot$). The data provide evidence for a sharp threshold in metallicity, above which SiC grains form with much higher $^{12}C/^{13}C$ ratios than below. Above this threshold, the fraction of grains with relatively high $^{12}C/^{13}C$ decreases exponentially with increasing $^{29}Si/^{28}Si$ ratio. This result indicates a sharp increase in the maximum mass of SiC parent stars with decreasing metallicity, in contrast to expectations from Galactic chemical evolution theory. *Copyright © 2003 Elsevier Ltd*

1. INTRODUCTION

Isotopic measurements of micron-sized materials traditionally have been sparse, because the relatively small number of atoms available limits the achievable measurement precision. However, scientific interest in the isotopic compositions of micron-sized dust grains has greatly increased in recent years, with the advent of highly sensitive measurement techniques (e.g., secondary ion mass spectrometry [SIMS]) and the discovery of relatively large isotopic variations in some micrometric materials. For example, primitive meteorites contain a tiny fraction of mineral grains with highly unusual isotopic compositions, compared to any other meteoritic or terrestrial materials. These presolar grains are believed to have originated in the cooling outflows from ancient stars and supernova explosions before the formation of the solar system. Since their discovery in 1987, presolar grains have yielded a wealth of information on astrophysical and cosmochemical processes (see, e.g., Anders and Zinner, 1993; Zinner, 1998; Nittler, 2003). Additional interest in isotopic measurements of small particles arises from the nuclear forensics community. For example, U and Pu isotopic compositions of particles sampled from nuclear enrichment facilities are used to monitor nuclear treaty compliance (Simons et al., 1998; Tamborini and Betti, 2000). Finally, there is recent interest in the isotopic composition of aerosol particles collected from the Earth's atmosphere (Aléon et al., 2002).

SIMS has been the most widely used analytical technique for measuring isotopic ratios in small particles, due to its high sensitivity and spatial resolution (Zinner, 1989; Zinner et al., 1989). Traditional SIMS measurements of single micron-sized particles are quite time-consuming, however, requiring a minimum of several minutes to locate a sample, align the primary beam with it, and analyze it. This relative inefficiency makes it difficult to obtain statistically significant datasets, especially for rare grain populations. Automated techniques in these cases are thus highly desirable.

Previously, direct ion imaging with Cameca ims-3f and ims-4f ion microprobes has been used with considerable success to automatically determine isotopic ratios in micron-sized particles (Nittler et al., 1994; Hoppe et al., 1996b; Nittler, 1996; Nittler et al., 1997; Simons et al., 1998; Hoppe et al., 2000). This technique exploits the stigmatic optics of the instrument: isotopic images of large areas of a sample can be transmitted and focused onto an imaging detector. Digitization of these images with subsequent image processing allows the determi-

* Author to whom correspondence should be addressed (lrn@dtm.ciw.edu).

nation of isotopic ratios in many particles simultaneously. This technique thus has the advantage of high data throughput and $\geq 10^3$ particles/day can be analyzed in an automated mode. However, ion imaging has significant limitations. For example, it is most useful for isotopic ratios that can be measured with relatively low ($M/\Delta M < 1000$) mass-resolving powers, e.g., D/H, $^{18}O/^{16}O$, $^{30}Si/^{28}Si$, and $^{235}U/^{238}U$. Increasing the mass resolution of the ion microprobe introduces optical aberrations into the ion images and decreases transmission of secondary ions, thus decreasing the signal-to-noise ratio. This precludes application of ion imaging to several isotopic ratios of interest, for instance $^{17}O/^{16}O$. Moreover, the precision for isotopic ratio measurements is apparently limited by inherent nonlinearity in the micro-channel plate image detector. For particles, the precision is several times worse than can be attained by traditional single-grain analyses.

To avoid the limitations of the ion imaging technique, we have developed a new analytical system for fully automated high-mass-resolution isotopic measurements of micron-sized particles using an ion microprobe. The system uses scanning (raster) ion imaging to locate particles dispersed on sample mounts, followed by grain-by-grain measurements. This article describes in detail the analysis system, and its current capabilities as reflected in the measurement of standards.

We also present an initial application of the system to meteoritic samples. We have analyzed Si and C isotopic ratios in ~ 3300 presolar silicon carbide (SiC) grains extracted from the Murchison meteorite. SiC is the best-studied presolar phase in meteorites. Silicon and carbon isotopic ratios have previously been reported for ~ 1500 individual grains (Alexander, 1993; Hoppe et al., 1994; Hoppe et al., 1996a; Huss et al., 1997), thus providing a large statistical base with which to compare the automatically acquired data. We have also used the large new SiC isotopic database to explore the relationships of the rare SiC Y and Z subgroups to the dominant mainstream population.

2. AUTOMATED PARTICLE ANALYSIS SYSTEM

2.1. Description of System

The particle measurement ("mapping") system is implemented on a Cameca ims-6f ion microprobe at the Carnegie Institution of Washington. It entails a number of steps: 1) One or more isotopic images are acquired by rastering a small (~ 1 μm) primary ion beam over a square area of a sample mount (typically ~ 75–150 μm square) containing dispersed particles. In all cases, particulate samples are deposited from isopropanol/water suspension onto clean Au foils. 2) An image-processing algorithm is used to identify individual particles in the images and returns the pixel coordinates of each grain. 3) The primary ion beam is deflected to and focused onto each grain in turn. 4) Each grain is analyzed for its isotopic composition, using a conventional peak-jumping technique. 5) Finally, once all the grains in an image have been analyzed, the sample stage is moved to a new position and the process is repeated. Each of these steps is described below.

The ims-6f ion probe includes a "dynamic-transfer optical system" (DTOS) for acquisition of rastered ion images. Voltages on deflection plates in the transfer optics of the instrument are synchronized with the primary ion beam raster in such a way that the secondary ion beam remains centered on the optical axis of the mass spectrometer, even for large primary beam deflections. By synchronizing the secondary ion detection with the primary ion raster, the original location of sputtered ions can be reconstructed, allowing secondary ion images to be acquired over large areas, even under high mass resolution conditions. The spatial resolution of the images depends solely on the primary beam diameter, which can be as small as 0.5 μm for the Cs^+ source and ~ 1 μm for the O^- source. Which primary ion source is used for a particular measurement depends on what is being measured, since different elements preferentially make negative or positive ions.

Before image acquisition of a given field of particles, the primary ion beam current is set to several nanoamperes and the beam is rastered over the area for 30–90 s. This presputtering removes adsorbed contamination and implants primary ions into the particles, greatly increasing the yield of secondary ions. The presputtering time and current are chosen empirically such that the C background is substantially reduced and particles produce sufficient secondary ions for detection in ion images. Following presputtering, the primary ion beam current is reduced to the measurement value (typically 10–50 pA) and the beam is centered on the optical axis of the mass spectrometer. This step is essential because the beam can shift as the sample stage is moved due to the non-normal incidence of the beam and surface topography of the sample. Centering is accomplished by scanning the beam across a 100-μm-diameter field aperture mechanically centered on the optical axis and finding the appropriate deflections to maximize the transmitted current. Because beam shifts for adjacent fields are typically smaller than the size of the field aperture, this method works very well.

After beam centering, scanning ion images are acquired for one or more species. For example, ^{28}Si or ^{12}C images, or both, are usually acquired to identify SiC grains in meteoritic acid-resistant residues. Image acquisition times are chosen such that sufficient counts are obtained for particles of a desired size to be identified by an automatic algorithm (see below) and are typically 1 to 2 min. Figure 1a shows an example of a ^{28}Si ion image of several synthetic SiC grains.

Particles are defined in scanning ion images using an algorithm previously developed for direct ion imaging studies (Nittler et al., 1997). Briefly, the algorithm first identifies potential particles by locating local intensity maxima in the images. Intensity profiles extending radially outward from each local maximum are then obtained, and neighboring pixels with intensities above a threshold (typically 35% of the maximum) are included in the defined particle. To distinguish close particles, only pixels for which the image intensity decreases monotonically in the radial direction away from the particle maximum are included in a given particle. Once all particles have been defined in an image, they are sorted according to preset criteria. For example, particles that are too close to each other to be reliably measured without cross-contamination are excluded as are particles that are either too large or too small. The final list of particles to be measured in an image is then returned to the measurement program. Shown in Figure 1b are contours indicating SiC particles defined in the image of Figure 1a; only those contours filled in gray survived the sorting process and were isotopically analyzed.

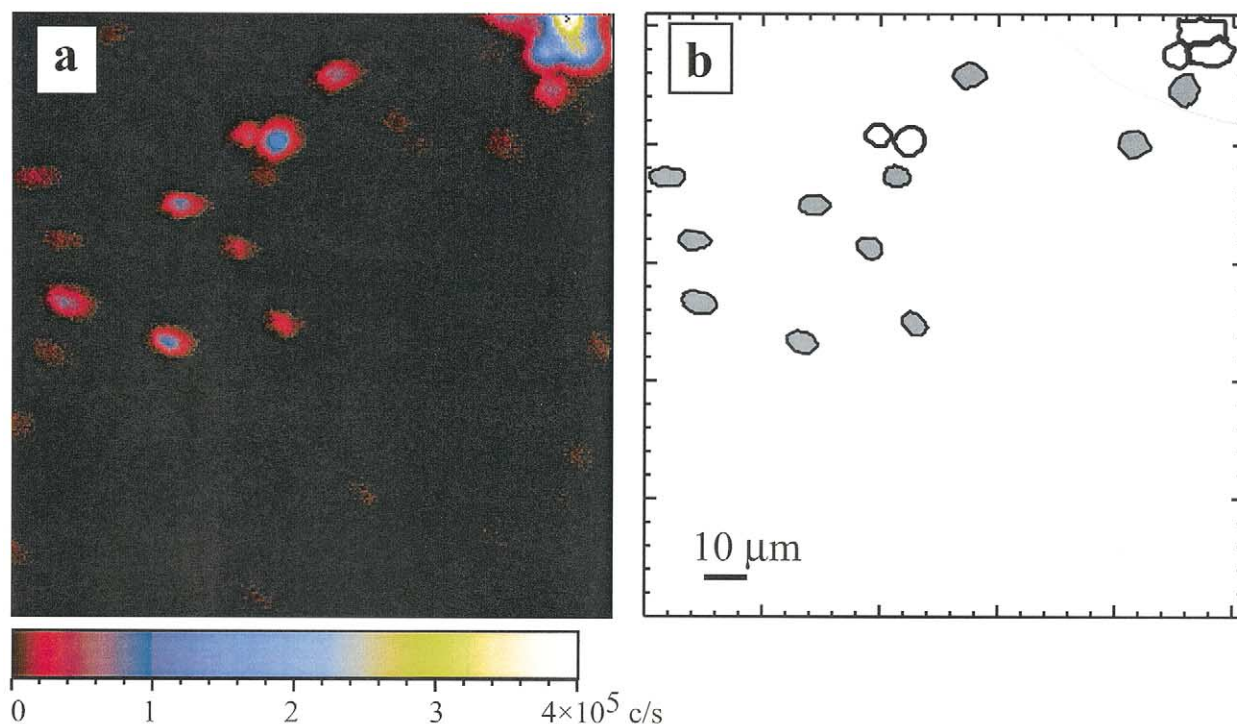In principle, defined particles could be analyzed either: (i) by

Fig. 1. (a) A false-color, $100 \times 100 \; \mu m$ scanning ion image ($^{28}Si^-$) of dispersed synthetic SiC grains. (b) Contours of particles identified in (a) by an automatic image processing algorithm. Filled contours indicate grains selected for isotopic analysis.

moving the sample stage to bring each one into alignment with the mass spectrometer optical axis, or (ii) by electrostatically deflecting the primary ion beam to each particle and using the DTOS to realign the secondary ion beam. Our system uses the latter method, because in the ims-6f, electrostatic deflection is much faster than accurate movement of the sample stage. This procedure requires use of transformation matrices both to relate pixel coordinates of particles in ion images to primary beam deflection voltages and to calculate appropriate secondary (DTOS) deflector voltages to compensate for specific primary beam deflections. An additional calibration matrix is used to determine sample stage coordinates for individual particles. These matrices are calculated by least-squares fitting to several points empirically determined in each coordinate system. Once the primary beam is deflected to a particle, it is next scanned over a few microns in x and y, and over an appropriate range of fine focus to maximize the secondary ion current. This ensures that the primary beam is properly centered and focused on the particle. At this point, the secondary count rate is also compared to a user-specified threshold; if it is below the threshold, the particle is not measured and the beam is deflected to the next particle in the list. Finally, a raster of $1–3 \; \mu m$ is applied to the primary beam (with the DTOS system energized). This decreases the sputter rate, helping to stabilize the secondary ion current. Also, it is our experience that rastering reduces mass fractionation variations due to geometric effects when using a finely focused ion beam on particles.

Once the primary beam is focused on a particle, the particle is measured for its isotopic composition using standard peak-jumping techniques (Zinner et al., 1989). Measurement details depend on the specific situation, but in all cases, the progress of the measurement is monitored every few cycles and stopped if certain preset criteria are met. For example, the user may select to stop a measurement once a specified statistical precision is reached or if the particle is sputtering away too fast (as indicated by rapidly decaying secondary ion count rates). Each defined particle in an image is measured in this way. The ims-6f magnet is sufficiently stable that drift of peak positions is usually small over hour time scales. Thus, to save time and minimize sputtering of particles, magnetic field settings for mass peaks are automatically centered only for the first particle analyzed in each image (always the brightest in the image).

After measurement of all particles in a given image, the sample stage is moved to an adjacent area, where the process is repeated. The sample is moved in a grid pattern with the size of the grid predetermined by the user. As originally configured, control of the ims-6f sample stage showed poor reproducibility (often $>50 \; \mu m$) in moving to specified locations. Because this was insufficient for automated analyses, a set of optical encoders was affixed to the stage and software was written to ensure reproducibility to $1 \; \mu m$.

The mapping system is incorporated into the general Lab-View (National Instruments) ion probe user interface originally supplied by Cameca with the instrument, running on a Sun Microsystems Ultra-10 workstation. Image processing is done using software written with the PV-WAVE programming language (Visual Numerics, Inc.). The PV-WAVE program runs in a server mode, waiting for commands and data sent by the LabView interface using a client program developed in C.
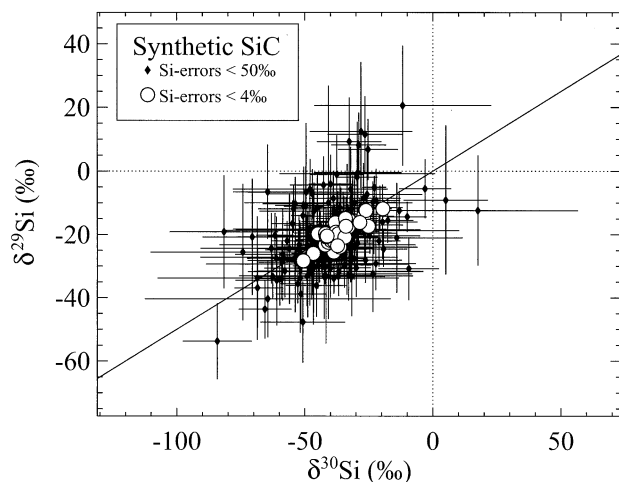
Fig. 2. Silicon isotopic ratios automatically determined in 234 synthetic 1–2-μm SiC grains, expressed as δ values: $\delta^i Si = 10^3 \times [(^i Si/^{28} Si)_{grain}/(^i Si/^{28} Si)_{Terrestrial} - 1]$, relative to the standard ratios of $^{29} Si/^{28} Si = 0.0506331$ (Barnes et al., 1975) and $^{30} Si/^{28} Si = 0.0334744$ (Zinner et al., 1989). Errors are 1σ and dotted lines indicate terrestrial ratios in this and subsequent figures. The data cluster around the slope $\frac{1}{2}$ mass-dependent instrumental mass fractionation line (solid line).

2.2. Measurements of Standards

To test the capabilities of the mapping system, Si and C isotopic compositions of 250 synthetic SiC grains were automatically obtained. The sample was nominally 2 μm in size, but in fact ranged in size from ~0.5 to 5 μm. Silicon-28 ion images were used to identify individual particles (Fig. 1). Isotopic measurements were made with a 50-pA, 1–2-μm diameter Cs^+ primary beam at a mass-resolving power of 3500, sufficient to resolve all interferences. Counting times per cycle were 1s, 3s, 1s, 5s, and 6s for ^{12}C, ^{13}C, ^{28}Si, ^{29}Si, and ^{30}Si, respectively.

Shown in Figure 2 are the Si-isotopic ratios for 234 grains with counting statistical errors for both $\delta^{29}Si$ and $\delta^{30}Si$ smaller than <50‰; the 31 grains with the highest precision (<4‰) are indicated separately. The high-precision data lie along the slope $\frac{1}{2}$ line expected for instrumental fractionation, with an average $\delta^{29}Si$ value of -19.9 ± 4.0‰ and an average $\delta^{30}Si$ value of -36.7 ± 6.5‰ (errors are one standard deviation). Since the standard has a true composition of $\delta^{29,30}Si = 0$‰, this indicates an average instrumental fractionation of ~-19‰/amu, which is quite typical for SIMS measurements of Si isotopes. The total uncertainty of a grain measurement is a combination of the counting statistical error and an intrinsic error due to variations in instrumental mass fractionation. The intrinsic error is the ultimate measure of the accuracy of the isotopic measurements, in the limiting case of negligible statistical error. The average statistical errors for the high-precision data in Figure 2 are 2.6‰ and 2.7‰ for $\delta^{29}Si$ and $\delta^{30}Si$, respectively. Assuming that the intrinsic and statistical errors add in quadrature, we thus estimate from the standard deviations of the high-precision measurements that the intrinsic uncertainty is ~3‰/amu for Si isotopic ratios. Binning all of the grain data by count rate and fitting the standard deviations of the bins as a function of count rate gives similar results. This
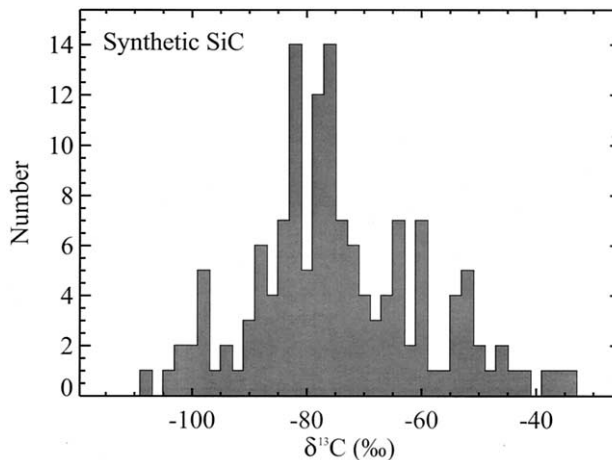

Fig. 3. Histogram of $\delta^{13}C$ values ($\delta^{13}C = 10^3 \times [(^{13}C/^{12}C)_{grain}/(^{13}C/^{12}C)_{Terrestrial} - 1]$) automatically determined in 141 synthetic SiC grains with individual measurement errors <20‰. The normalizing ratio is that of PDB ($^{13}C/^{12}C = 0.011237$). The true composition of the grains is $\delta^{13}C_{PDB} = -35$‰, indicating a typical instrumental mass fractionation of -43‰. The range of values is consistent with counting statistical errors.

reproducibility is close to that obtained by manual analyses of SiC grains (Zinner et al., 1989; Hoppe et al., 1996a; Huss et al., 1997) and indicates that the automated system introduces no significant additional uncertainty beyond that already present for SIMS measurements of particles.

The errors in $^{12}C/^{13}C$ ratios measured in the grains are larger than the Si errors, due to shorter counting times and the lower natural abundance of ^{13}C. A histogram of $\delta^{13}C$ values for 141 grains with errors less than 20‰ is shown in Figure 3. The range of measured composition is completely consistent with counting statistics. Considering a subset of 55 grains with uncertainty <10‰, we find an average value of $\delta^{13}C = -78.0 \pm 7.6$‰. This error is dominated by counting statistics, so it is not possible to accurately estimate the intrinsic error as was done for Si isotopes. The synthetic SiC has $\delta^{13}C_{PDB} = -35$‰, indicating an average instrumental fractionation of -43‰ and a reproducibility better than 8‰. Again, this is similar to manual SiC analyses, indicating that the automated analyses introduce no additional uncertainty.

Figure 4 shows the measured $\delta^{29}Si$ values for 234 grains with errors <20‰, plotted as a function of distance from the optical axis. The dashed line indicates the average value for the dataset. Clearly, there is no dependence of the measured isotopic composition on the primary beam deflection. Within the precision of the measurements, the DTOS correctly compensates for large primary beam deflections.

Figure 5 shows O isotopic ratios determined automatically in 89 terrestrial Al_2O_3 grains with approximate sizes of 1–2 μm. Individual grains were identified in 100×100 μm ^{16}O images. A 30-pA Cs^+ beam was used for isotopic measurements, with a mass resolving power of 5000, sufficient to resolve ^{16}OH from ^{17}O. Negative secondary ions of ^{16}O, ^{17}O, ^{18}O, and $^{27}Al^{16}O$ were collected with counting times of 1s, 8s, 4s, and 0.5s, respectively. AlO^- was included to monitor whether analyzed grains were indeed Al_2O_3, rather than O-bearing contamination sometimes found on sample mounts. A total of

2.3. Efficiency
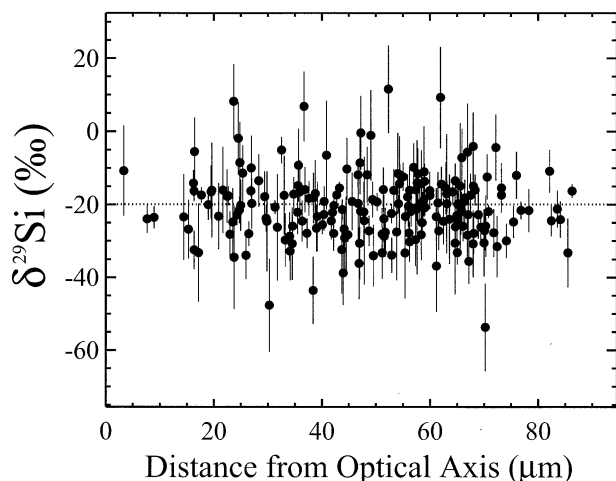
Because the mapping system analyzes particles sequentially, its efficiency is lower than the previously used direct ion imaging technique (see Section 1). The rate at which particles are analyzed depends on the specific analysis conditions, grain sizes and density on sample mounts, and the desired statistical precision. For the studies described here, we have achieved typical rates of ~300 analyzed particles/day, indicating an average measurement time of about 5 min per particle. This efficiency could be increased up to ~1000 particles/day, if only low-precision data (e.g., >50‰ statistical uncertainty) were required and the grain density was optimized (>20 particles per image). Implementing this system on an ion probe with multiple detection capabilities could also greatly increase the efficiency.

3. METEORITIC SiC: SAMPLES AND EXPERIMENTAL TECHNIQUES

Two SiC-rich acid residues of the Murchison CM2 chondrite were used for this study. The first was prepared using the standard procedures reported by Amari et al. (1994); previous Si and Ti isotopic data from this residue were reported by Alexander and Nittler (1999). The second was prepared from an aliquot of an insoluble organic residue of Murchison (Cody et al., 2002). For this residue, CsF was used for the digestion of silicate minerals in contrast to the conventional HF technique. A saturated solution of CsF (~30M) is strongly alkaline and its density is ~2.7 g/cc. To prepare the salt solution, water and concentrated HF were added to produce a pH of 5–6 and a density of ~1.7 g/cc. The demineralization was carried out in the presence of two immiscible liquids: the aqueous fluoride salt solution and a dioxane-CS_2 mixture. The sample, salt solution and dioxane-CS_2 mixture were combined in a tightly capped Teflon tube and shaken. Liberation of the organics begins within hours. Because of the density of the salt solution, upon standing, the organics float up to the interface of the immiscible liquids, while the more dense material sinks to the bottom. The liberated organics are extracted after centrifugation and then washed in a ~1:1:1 mixture of dioxane–CS_2–water. HCl (HCl ~1M) was added to remove CsF and any other soluble material. Dioxane and CS_2 were used to remove any elemental S.

Small particulates (typically <10 μm) tend to be trapped by the organic material. Some silicates can survive CsF, and the organic residue was briefly treated with 9 mol/L HF/1 mol/L HCl. To remove the organics, chromite, etc., the sample was then oxidized with perchloric acid at ~200°C. The remaining sample was centrifuged and washed. Nanodiamonds were extracted from the sample with a ~0.1 mol/L NH_4OH solution combined with centrifugation. To concentrate grains of the desired size range, a ~1–5 μm size separate was prepared by settling in a ~50:50 mix of water and isopropanol. The dominant mineral in the residue at this stage was spinel. To increase the fraction of SiC and reduce the potential for overlap with spinel grains, the sample was treated several times with concentrated H_2SO_4 at ~200°C (Amari et al., 1994). The final step was to treat the sample with HF/HCl to remove any oxide layer that had developed on the SiC.

Si and C isotopic ratios were automatically determined for SiC grains from two mounts of the first Murchison residue and from three mounts of the second residue. All samples were size-separated by centrifugation with a nominal size range of 1–5 μm. Most of the sample mounts were ashed in an O plasma before isotopic analysis to remove surface organic contamination. The isotopic measurement conditions were the same as described above for synthetic SiC analyses (Section 2.2), except that $^{16}O^-$ was added to the mass list for some measurements to check for silicate contamination. Standards were measured before mapping each mount to determine instrumental fractionation. Because small grains sputter quickly under the focused beam, a correction for decreasing count rates was necessary. Individual cycle isotopic ratios were computed by linearly interpolating the count rate of the major isotope between two successive cycles. This correction is of course most severe for the smallest grains. For grains analyzed here of

Fig. 4. Delta-^{29}Si values plotted against distance from the optical axis of the mass spectrometer for 234 synthetic SiC grains analyzed automatically. The lack of correlation between these quantities indicates that the dynamic transfer optical system (DTOS) of the ims-6f correctly compensates for large primary ion beam deflections.

150 corundum grains were measured, but for clarity, only the grains with individual statistical errors less than 10% are included in Figure 5. Taking averages of the 36 measured grains with errors less than 20‰, we find $\delta^{17}O = -13.3 \pm 15.5‰$ and $\delta^{18}O = -25.0 \pm 9.7‰$ (errors are dominated by counting statistics). As for Si, the data cluster around a slope ½ line reflecting mass-dependent instrumental fractionation. Because of the relatively large statistical errors, we are unable to estimate the intrinsic uncertainty for O-isotopic measurements as was done above for Si. However, the estimated reproducibility from these measurements (10–15‰) is both consistent with counting statistics and sufficient to identify presolar grains, whose O-isotopic ratios differ from standards by hundreds to thousands of permil.
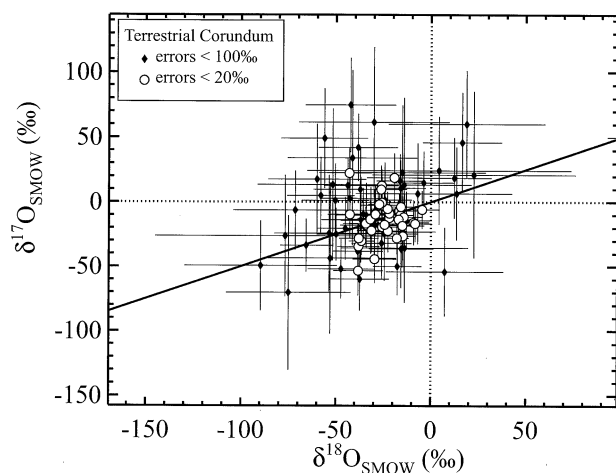

Fig. 5. O isotopic ratios, expressed as δ values relative to the SMOW standard, automatically determined in 89 terrestrial 1–2-μm Al_2O_3 grains. The data cluster around a slope ½ instrumental mass fractionation line. The measurement precision is sufficient to identify presolar oxide grains.

Table 1. Murchison SiC grain mounts analyzed in this study.

Mount	Dissolution method	Analyzed grains
M8	Standard	276 SiC
M10	Standard	68 SiC
M-3-3	CsF	938 SiC; 2 Si_3N_4
M-2-6	CsF	1796 SiC
M-4-2	CsF	265 SiC; 1 Si_3N_4

~1 μm diameter, the interpolation resulted in typical corrections of 5–50‰ for $\delta^{29}Si/^{28}Si$, 10–100‰ for $\delta^{30}Si/^{28}Si$, and 0–100‰ for $\delta^{13}C/^{12}C$. Grains of 0.5 μm had corrections to $\delta^{30}Si$ values as high as 200‰. The good agreement between our data and previous measurements of presolar SiC (Section 5) indicates that the count rate interpolation correction was applied correctly.

Errors for grain measurements are based on the quadratic sum of the standard error of the mean of individual cycle measurements and the external reproducibility of standards. Because the measured $\delta^{29}Si$ and $\delta^{30}Si$ values for standard grains spread out along a slope ½ instrumental fractionation line (Fig. 2), errors in these ratios for the SiC measurements are correlated. This results in error bars for individual grains not being aligned with the coordinate axes (e.g., Figs. 7, 11, 13), as described by Virag et al. (1992). This is only significant for the grains with the smallest counting statistical errors, however.

The numbers of analyzed SiC grains from each mount are detailed in Table 1. An additional 745 measured grains are excluded from the discussion because (i) they had Si/C ratios outside the range observed in synthetic SiC, (ii) their isotopic composition was within two sigma of solar in all three measured isotope ratios, or (iii) the errors from their Si isotopic measurements were greater than 60‰ (most measurements had errors smaller than 20–30‰). Three presolar grains of silicon nitride (Si_3N_4) were also identified and analyzed on the sample mounts.

The sizes of individual measured grains for mounts M-3-3 and M-2-6 were estimated by assuming that the diameter is proportional to the square root of the $^{28}Si^-$ count rate at the beginning of the measurement (Hoppe et al., 1996a). The appropriate proportionality constant was determined for each mount by re-finding a number of measured grains in a scanning electron microscope. The uncertainty in the size determined in this way is ~30%, based on scatter of the calibration grains.

4. METEORITIC SiC: RESULTS

A comma-separated variables text file containing the Si and C isotopic data for the 3343 SiC grains and three Si_3N_4 grains from Murchison is available as an electronic supplement on the Elsevier World Wide Web page.

The estimated grain size distribution for the 2734 measured grains from mounts M-2-6 and M-3-3 is shown in Figure 6. The grains range in diameter from ~0.5 to ~4 μm, with mean and median values of 1.0 μm and 0.9 μm, respectively.

Si isotopic ratios, expressed as δ values, for the analyzed SiC and Si_3N_4 grains are shown in Figure 7. Delta-^{29}Si values range from –550‰ to +200‰ ($^{29}Si/^{28}Si$ = 0.4–1.2 times solar), and $\delta^{30}Si$ values range from –700‰ to +1100‰ ($^{30}Si/^{28}Si$ = 0.3–2.1 times solar, with all but one grain having $\delta^{30}Si$ < 300‰). Mass-weighted averages are $<\delta^{29}Si>$ = 35.8 ± 0.7‰ and $<\delta^{30}Si>$ = 41.8 ± 0.7‰. As is well established for meteoritic SiC, most grains lie in the upper-right, $^{29,30}Si$-rich quadrant (the "mainstream" population, Hoppe and Ott, 1997). Also clearly visible on this plot are the rare ^{28}Si-rich X grains and related Si_3N_4 grains (Amari et al., 1992; Nittler et al., 1995; Hoppe et al., 2000; Besmehn and Hoppe, 2003) and the ^{30}Si-rich, ^{29}Si-poor Z grains (Alexander, 1993; Hoppe et al., 1997). One unusual grain, M26a-454-3, is extremely enriched in ^{30}Si,
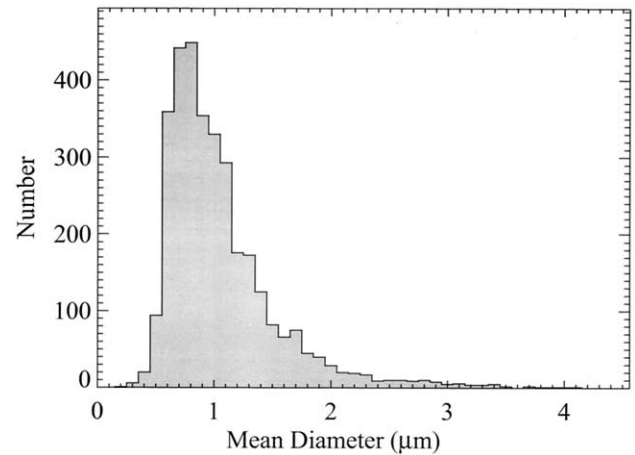

Fig. 6. Estimated grain size distribution of 2734 presolar SiC grains measured on mounts M-3-3 and M-2-6. Grain diameters range from ~0.5 to 4 μm, with a mean size of 1.0 μm.

with a more modest ^{29}Si enrichment ($\delta^{29}Si$ = 79 ± 13‰, $\delta^{30}Si$ = 1056 ± 38‰). Subgroups will be discussed in more detail below.

A histogram of measured C-isotopic ratios for the SiC grains is shown in Figure 8a, and is compared with the distribution from previous studies in Figure 8b. The grains have $^{12}C/^{13}C$ ratios that range from 2 to 4000. Similar to previous observations, most grains are enriched in ^{13}C, with a mass-weighted mean $^{12}C/^{13}C$ ratio of 37.9 ± 0.8 and a median value of 49.6. The present distribution is very similar to the previous data; but minor differences exist, as discussed in detail in Section 5.

With only a few minor exceptions, the Si and C data are sufficient to assign a given grain to one of the subgroups that have been defined for presolar SiC over the last decade. The different groups are indicated in Figure 9, where $\delta^{30}Si$ is plotted versus $^{12}C/^{13}C$ ratios for the measured grains. Our
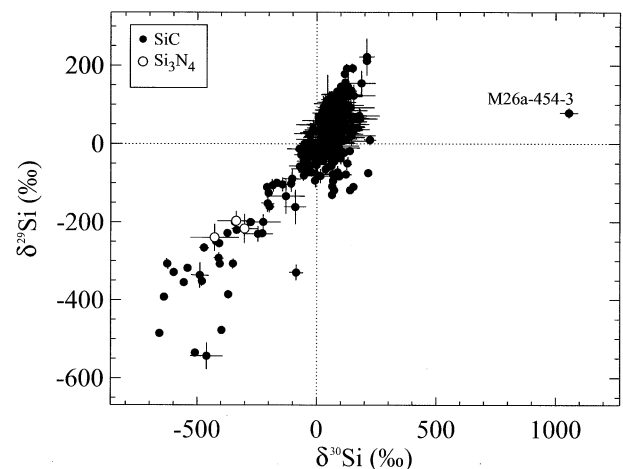

Fig. 7. Silicon isotopic ratios of 3343 presolar SiC and three Si_3N_4 grains from the Murchison meteorite. Most grains are enriched in the heavy Si isotopes, though the ^{28}Si-rich X grains and ^{30}Si-rich, ^{29}Si-poor Z grains are clearly visible. One grain, M26a-454-3, has a very high $^{30}Si/^{28}Si$ ratio and a more modest ^{29}Si excess.
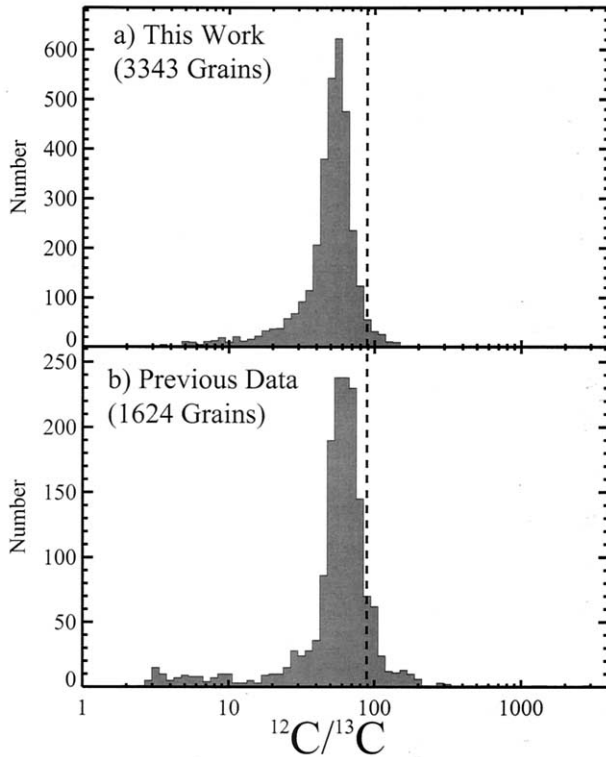
Fig. 8. Histograms of $^{12}C/^{13}C$ ratios measured in presolar SiC grains from meteorites: (a) 3343 Murchison grains from this study, (b) 1624 previously studied grains from Murchison (Hoppe et al., 1994; Hoppe et al., 1996a), Orgueil (Huss et al., 1997), and enstatite and ordinary chondrites (Alexander, 1993). The vertical dashed line indicates the terrestrial ratio of 89. Most grains are enriched in ^{13}C, with median $^{12}C/^{13}C$ of 50 (a) and 56 (b).

definitions for the groups basically follow those of Hoppe and Ott (1997) and are summarized, together with their relative abundances in Table 2. Following Amari et al. (2001c), we do
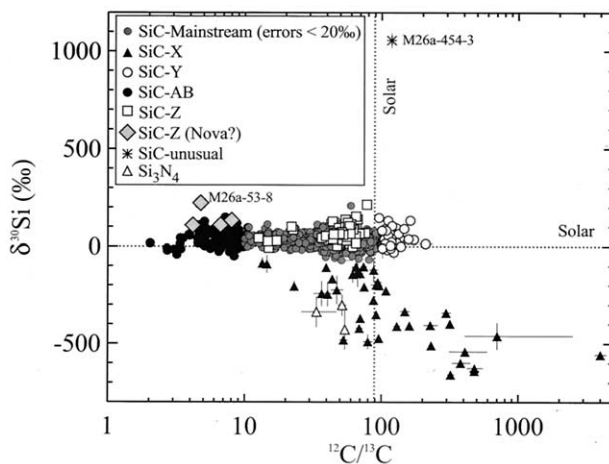

Fig. 9. Delta-^{30}Si values plotted against $^{12}C/^{13}C$ ratios for presolar SiC and Si_3N_4 grains of this study. Different symbols indicate classification into subgroups, according to Table 2 and Hoppe and Ott (1997).

not distinguish between the low $^{12}C/^{13}C$ ratio groups A and B and instead combine them into one group, here called AB. In some cases, unambiguously assigning a grain to a specific group is not possible. For example, some grains with Z-grain Si isotope signatures also have AB-grain C isotopic ratios. These grains are in fact classified here as being of type Z, but are discussed below as possible nova condensates. Nitrogen isotopic measurements would help clarify the classification (and origin) of these grains.

5. METEORITIC SiC: COMPARISON WITH PREVIOUS DATA

5.1. Overall Comparison

Because presolar SiC is quite well studied, we can use the large preexisting database of presolar SiC isotopic data as a standard with which to compare the present data. For comparison, we consider here the datasets of Hoppe et al. (1994, 1996a) for Murchison (CM2) SiC (KJE, KJG, and KJH separates of Amari et al., 1994), Huss et al. (1997) for Orgueil (CI) SiC, and Alexander (1993) for SiC from enstatite and ordinary chondrites. The average size of our grains is similar to that of the KJE Murchison SiC separate (1.14 μm), but includes several hundred grains of similar size to the larger KJF, KJH, KJH Murchison separates. The previous studies found little evidence for systematic differences in Si or C isotopic compositions for presolar SiC grains from different meteorites or as a function of grain size, so we combined the data into one large database containing ~1600 C isotopic measurements and ~800 Si isotopic measurements. Data from additional studies are compared below when we discuss the various SiC subgroups separately.

To first order, the present results are very similar to previous observations of presolar SiC, both in the range of C and Si isotopic compositions and in the isotopic systematics and abundances of the various subgroups. For example, the mass-weighted averages of C and Si isotope ratios of the present data overlap within errors the averages found in previous studies (e.g., Hoppe et al., 1996a; Amari et al., 2000). As for the measurements of terrestrial standards (Section 2), this indicates that the mapping system indeed accurately measures isotopic ratios in micron-sized particles and allows the automatic identification of rare subpopulations. However, there are some minor but significant differences in detail between the automatic data and the previously reported data. In particular, the C isotopic distributions differ in the following respects: (i) the median $^{12}C/^{13}C$ ratio of the present data is 50, compared to 56 for the previous data; (ii) the present dataset has fewer grains with very low $^{12}C/^{13}C$ ratios (2.8% have $^{12}C/^{13}C$ < 10, compared to 6.1%) and more grains with 10 < $^{12}C/^{13}C$ < 20 (4.2% compared to 1.9%); and (iii) we see fewer grains with $^{12}C/^{13}C$ >100 (1.9% compared to 5.0%).

There are several possible explanations for the C isotopic differences between the present and previous datasets. First, it could be due to some unrecognized instrumental artifact of the automated measurement technique. We find this highly unlikely, because the mapping system gives identical results to manual single-grain analysis for isotopic standards (Section 2). Second, since for the present measurements the ion beam was rastered over an area larger than the grain, terrestrial contamination from the sample substrates could have contributed to

Table 2. Groups of presolar SiC grains.

Group	Definition	Abundance (%)	Abundance (Hoppe and Ott, 1997)
Mainstream	$^{12}C/^{13}C = 10–100$ (excluding X and Z)	93	87–94
AB	$^{12}C/^{13}C < 10$	2.8	4–7
Y	$^{12}C/^{13}C > 100$ (excluding X)	1.5	1–2
Z	$\delta^{29}Si < 0$; ^{30}Si-rich side of mainstream line	1.4	≤3
X	$\delta^{29,30}Si < -100‰$	1.2	1

the analyses. This would affect grains with high $^{12}C/^{13}C$ ratios the most and might play a role in the lower fraction of grains with isotopically light C in the present data (point iii, above). However, it would not explain a shift of the bulk of the distribution towards lower $^{12}C/^{13}C$ ratios (point i), and an unreasonably large contribution would be required to explain the lack of grains with very low $^{12}C/^{13}C$ ratios. Also, the Si/C ratios of the grains were very similar to those found in previous studies, but a higher contamination background of C than of Si is typical. Finally, the average Si-isotopic ratios lie within the range of previous studies with no hint of mixing with terrestrial contamination.

Qualitatively, several of the observed differences in C isotopic distributions could be explained if many of the present measurements were not, in fact, of single grains, but rather of aggregates of grains lying too close to each other on the sample mounts to be distinguished by the ion images. Such aggregation would tend to squeeze the $^{12}C/^{13}C$ ratio distribution towards the mass-weighted average, shifting the median value lower, and shifting grains with extremely low (high) $^{12}C/^{13}C$ ratios higher (lower). We think that this is unlikely to explain all of the differences, since scanning electron microscopy (SEM) investigation of the grain mounts indicated that individual grains were mostly well separated. Moreover, grain mount M-2-6 was significantly more crowded than the other analyzed mounts, yet we see no significant differences in the isotopic data for this mount compared to the others. Nonetheless, some aggregation is unavoidable when depositing samples on substrates. To see how much aggregation would be required to explain the C isotope differences, we generated synthetic isotopic distributions. In each case, we generated compositions for 10,000 "measurements," where each measurement was assumed to be an aggregate of n grains taken randomly from the previous SiC dataset. The value of n was first chosen to be constant for all measurements in a distribution. In this case, $n = 5$ is required to explain a shift in median $^{12}C/^{13}C$ ratio from 56 to 50, but the resulting distribution has essentially no grains with $^{12}C/^{13}C$ <10 or >100. We next tried a more realistic model where, for each measurement, n was taken as $n' + 1$, where n' was selected from a Poisson distribution with mean value μ. For example, if $\mu = 1$, then 36% of the resulting measurements are single grains, 37% are aggregates of two grains, 19% are three grains, and the remainder are larger aggregates. We find that a value $\mu = 0.7$ is required to shift enough grains with low $^{12}C/^{13}C$ ratios into the range of 10–20 to match the data (point iii above). In this case, half of all measurements are aggregates of two or more grains. However, with this value, the median $^{12}C/^{13}C$ ratio is hardly shifted (from 56.5 to 55.5) and the fraction of grains with $^{12}C/^{13}C$ > 100 is

3.3%, still higher than observed. To shift the median $^{12}C/^{13}C$ ratio from 56.5 to 50.0 requires $\mu \sim 4.5$; with this value, only 1% of the measurements are actually single grains and again no measurements with very high or low $^{12}C/^{13}C$ ratios are expected. It thus appears that grain aggregation cannot quantitatively account for all of the differences in C isotopic distributions between the previous and present SiC datasets, especially the lower median $^{12}C/^{13}C$ ratio of our data. This also holds for the Si isotopic data, because aggregation would shrink the distribution of Si isotopic ratios about the mean values, but we observe a similar range of ratios to previous work.

A final explanation for the isotopic differences between our data and that of previous studies is that the differences are real. Ninety percent of the new SiC measurements were from samples prepared using fundamentally different chemical techniques than the Chicago procedures, used for all previous studies (e.g., Amari et al., 1994). SEM images of SiC grains extracted using the Chicago methods typically have very pitted surfaces, almost certainly due to attack during sample preparation since surfaces of nonetched SiC grains are much cleaner (Bernatowicz et al., 2000). We have not explored the effects of the new CsF chemistry on SiC grain morphology, but in general the processing appears to be gentler than the Chicago procedures. For example, in this study we found three Si_3N_4 grains among 3000 SiC grains. Although statistics are poor, this is a factor of 3 higher than the ratio Nittler et al. (1995) found in the Murchison KJG SiC separate, indicating that Si_3N_4 survives the new treatment better. It is possible that the standard chemical extraction techniques slightly modify the isotopic compositions of the SiC grains, for example by isotopic exchange. More likely, there could be some SiC grains within the presolar population that are more fragile than others, perhaps due to structural defects, and are preferentially destroyed by the standard acid treatments. If these grains had subtly different isotopic characteristics (due, for example, to formation in a different population of stars), this could in principle explain the observations.

Shown in Figure 10 are histograms of $^{12}C/^{13}C$ ratios for our SiC grains, divided into the grains isolated using CsF and those isolated using the traditional HF/HCl treatments. Also shown is a histogram of the SiC data from previous work. The HF/HCl histogram is in close agreement with that of previous studies, but the main CsF distribution is clearly skewed towards lower $^{12}C/^{13}C$ ratios. Because all of our data were acquired using the same automated method on the same instrument, this result strongly supports the assertion that the observed difference in $^{12}C/^{13}C$ distribution between our data and previous work is real and related to the different chemical treatments used. On the other hand, there is no significant difference in the distribution
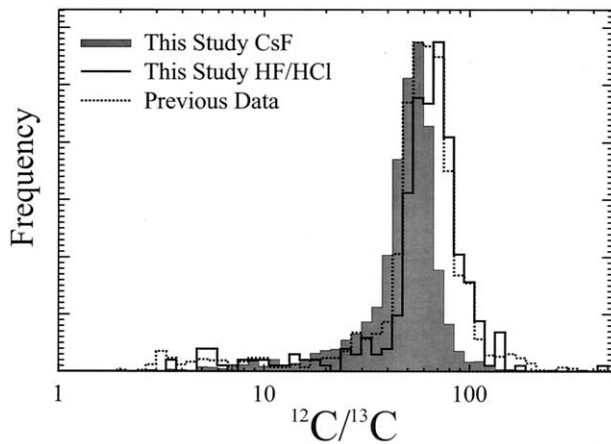
Fig. 10. Distributions of $^{12}C/^{13}C$ ratios for the 2999 SiC grains of this study isolated using the new CsF technique (shaded histogram), 344 grains isolated using the HF/HCl method (solid line), and 1624 grains from previous studies (dotted line, see Fig. 8 for references). Histograms are normalized so that their maximum values match on plot. The bulk of the CsF distribution is clearly shifted to ^{13}C-rich compositions relative to the grains isolated using HF/HCl, both from this study and prior work, suggesting that there is a population of SiC grains that is preferentially destroyed using the traditional chemical dissolution methods.

of Si isotopic ratios between the grains isolated using CsF and those isolated using traditional methods. Comparative transmission electron microscopy of SiC grains isolated by the different chemical or physical techniques could help confirm this suggestion that a large fraction of meteoritic grains are destroyed using the standard methods. Also, it is possible to locate presolar SiC grains without any chemical dissolution of the parent meteorite using SEM techniques (Alexander et al., 1990; Bernatowicz et al., 2000; Stroud et al., 2002). Isotopic measurements of a large number of grains could determine the "true" C-isotope distribution of presolar meteoritic SiC. Finally, it is worth noting that the large SiC grains measured by Virag et al. (1992) from the Chicago L-series separates had isotopic systematics quite distinct from the SiC datasets discussed here, indicating some level of heterogeneity in Murchison SiC.

In summary, although some of the differences between the overall C isotopic distribution reported here and those of previous SiC studies are likely due to contamination or grain aggregation, or both, we think that the bulk of the difference is probably intrinsic to the samples. In the remainder of this section we shall compare our data with previous results for the various subgroups in detail.

5.2. Mainstream SiC

Some 90% of presolar SiC grains belong to the mainstream population, with $^{12}C/^{13}C$ ratios in the range 10–100 and $\delta^{29,30}Si$ values ranging from $\sim$ –50‰ to $\sim$ +200‰, clustering near a line of slope $\sim$1.3 on the Si 3-isotope plot. As discussed in more detail in Section 6, these grains most likely originated in the winds of low-mass C-rich asymptotic giant branch

(AGB) stars. Figure 11a shows Si δ values for 1897 mainstream grains from the present study with errors < 20‰; 357 grains with errors less than 10‰ are indicated by open symbols. Data for 570 grains (errors < 20‰) from previous studies are shown for comparison in Figure 11b. As for the overall comparison discussed above, there is good agreement in the overall range of compositions between the new and previous data. One new grain has a more extreme $^{29,30}Si$ rich composition ($\delta^{29,30}Si \sim$ +200‰) than previously observed; an additional grain was found with a similar composition, but larger errors (Fig. 7). A weighted least-squares fit (solid line) to the combined (old + new) dataset of 688 grains with errors <10‰ has a slope of 1.35 ± 0.01 and an intercept of –18.3 ± 0.6. Fitting the datasets separately gives essentially identical results. The only fundamental difference appears to be the absence of grains in our dataset with $\delta^{29}Si \sim$ 170‰, clearly present in Figure 11b (ellipse). Most of these grains were identified in an Orgueil acid residue by Huss et al. (1997) and found to fall into two sets of closely similar C-isotopic ratios. Huss et al. defined these grains to belong to two groups, called V and VI, and suggested that they originated in two individual parent stars. Regardless of their origin, these grains are much less abundant in Murchison than in the Orgueil sample of Huss et al. Considering the 10 grains within the ellipse in Figure 11, six are from Orgueil, three are from previous Murchison studies, and one is from the present study, corresponding to relative abundances of 4.3%, 0.7%, and 0.05%, respectively.

To investigate whether there are preferred compositions along the mainstream SiC Si-isotope array, Huss et al. (1997) calculated error-weighted histograms of $^{29}Si/^{28}Si$ ratios (their Fig. 3) for their Orgueil sample as well as the Murchison KJE, KJG, and KJH SiC data from Hoppe et al. (1994, 1996a). We have performed a similar exercise, because we now have a much larger dataset with relatively precise isotopic measurements. We computed a two-dimensional probability distribution for 688 grains (both previous and new data) for which analytical errors in their Si-isotopic ratios were less than 10‰. The distribution is a sum of unit-area 2-d Gaussian distributions, where each Gaussian is centered on the $\{x,y\} = \{\delta^{30}Si, \delta^{29}Si\}$ value for a specific grain and the semimajor and semiminor axes are determined from the grain's analytical uncertainties. Results are shown as a contour plot in Figure 12a and as a shaded surface plot in Figure 12b. There are two prominent peaks, roughly centered at $\{\delta^{30}Si, \delta^{29}Si\} = \{30, 20\}$ and $\{50, 50\}$, as well as a number of smaller peaks. The Group V and VI grains are visible as a small peak at $\{170, 140\}$. The peak at $\delta^{29,30}Si \sim$ 50‰ is actually partially resolved into two peaks, with centers at $\{43, 41\}$ and $\{52, 49\}$, respectively. The latter peak was prominent in the Orgueil data of Huss et al. (1997). About half of the Orgueil grains with this Si-isotopic composition also had $^{12}C/^{13}C$ ratios $\sim$63. Huss et al. called these Group IV grains. Although these grains are clearly present in Murchison as well, we estimate their abundance in this meteorite to be $\sim$1.5% of the total SiC, much lower than the 8% fraction found in Orgueil. None of the other peaks in the probability distribution show obvious clustering in their $^{12}C/^{13}C$ ratios, and thus they probably do not correspond to grains from a single star, as suggested for the groups IV, V, and VI by Huss et al. (1997).

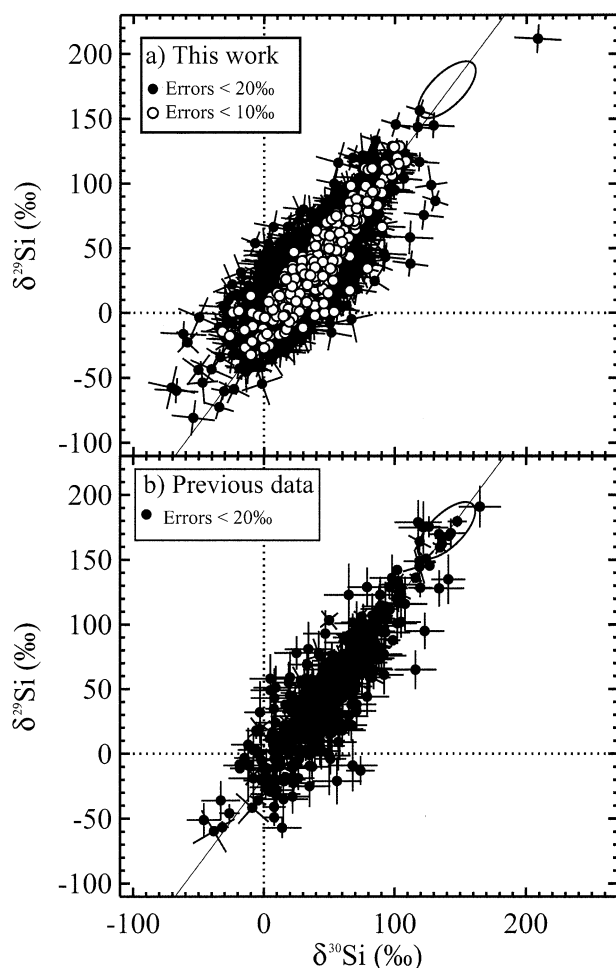Clearly, most of the differences we see between our data for

Fig. 11. Si-isotopic ratios, expressed as delta values for mainstream SiC grains: (a) 1897 grains from the present study with errors in both $^{29}Si/^{28}Si$ and $^{30}Si/^{28}Si$ smaller than 20‰; open symbols indicate grains with errors smaller than 10‰. One grain is more enriched in the heavy Si isotopes than any previously observed mainstream grains. (b) 570 grains from previous studies (see Fig. 8 for references) with errors <20‰. The solid line indicates the best-fit line to the 688 grains from both panels with errors smaller than 10‰: $\delta^{29}Si = -18.3 + 1.35 \cdot \delta^{30}Si$. Ellipse indicates a cluster of grains observed in an Orgueil acid residue (Huss et al., 1997), but not present in the large Murchison database presented here.
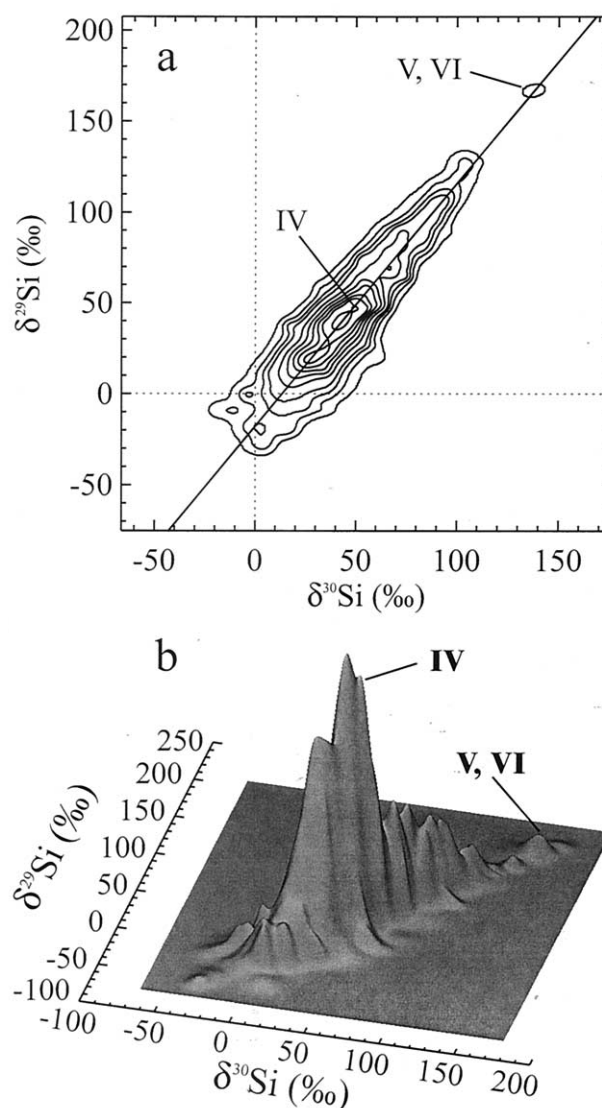

Fig. 12. Probability distribution of mainstream SiC Si-isotopic compositions generated by summing Gaussian distributions corresponding to measurement uncertainties for individual grains. (a) Contour plot of probability distribution. The solid line is the best-fit line to the mainstream grains (Fig. 11). (b) Shaded surface representation of distribution. The location of grain groups IV, V, and VI, defined by Huss et al. (1997) are indicated; groups V and VI were not seen in the present study (Fig. 11) and group IV has a much a lower abundance in Murchison than in Orgueil data of Huss et al. (1997).

mainstream SiC from Murchison and the previous data are absence or lower abundances of the grain groups defined by Huss et al. (1997). We note that this difference is not due to grain size. Although most of our grains were smaller than the Orgueil grains, our dataset still includes ~200 grains larger than 1.5 μm, comparable to the 140 grains measured by Huss et al. It is possible that the different abundances of the grain groups indicate that the parent bodies of Orgueil and Murchison accreted differing populations of SiC grains, but this seems unlikely given the very similar abundances of different presolar grain types in all types of chondrites (Huss and Lewis, 1995). More likely, we think the differences are statistical in nature, owing to the relatively small numbers of grains analyzed in the Huss et al. (1997) study.

5.3. AB Grains

AB SiC grains are defined as having $^{12}C/^{13}C$ ratios <10 (Table 2, Hoppe and Ott, 1997; Amari et al., 2001c). We found 90 AB grains in our study, corresponding to an abundance of 2.7%, smaller than the 5% abundance found in earlier studies. As discussed earlier in Section 5.1, some, but not all, of this difference is attributable to terrestrial contamination or grain aggregation on sample mounts. The Si isotopic ratios for the 90 new AB grains are shown in Figure 13a. Also shown for comparison are the compositions of previously identified AB grains and mainstream SiC grains. The new data are in very
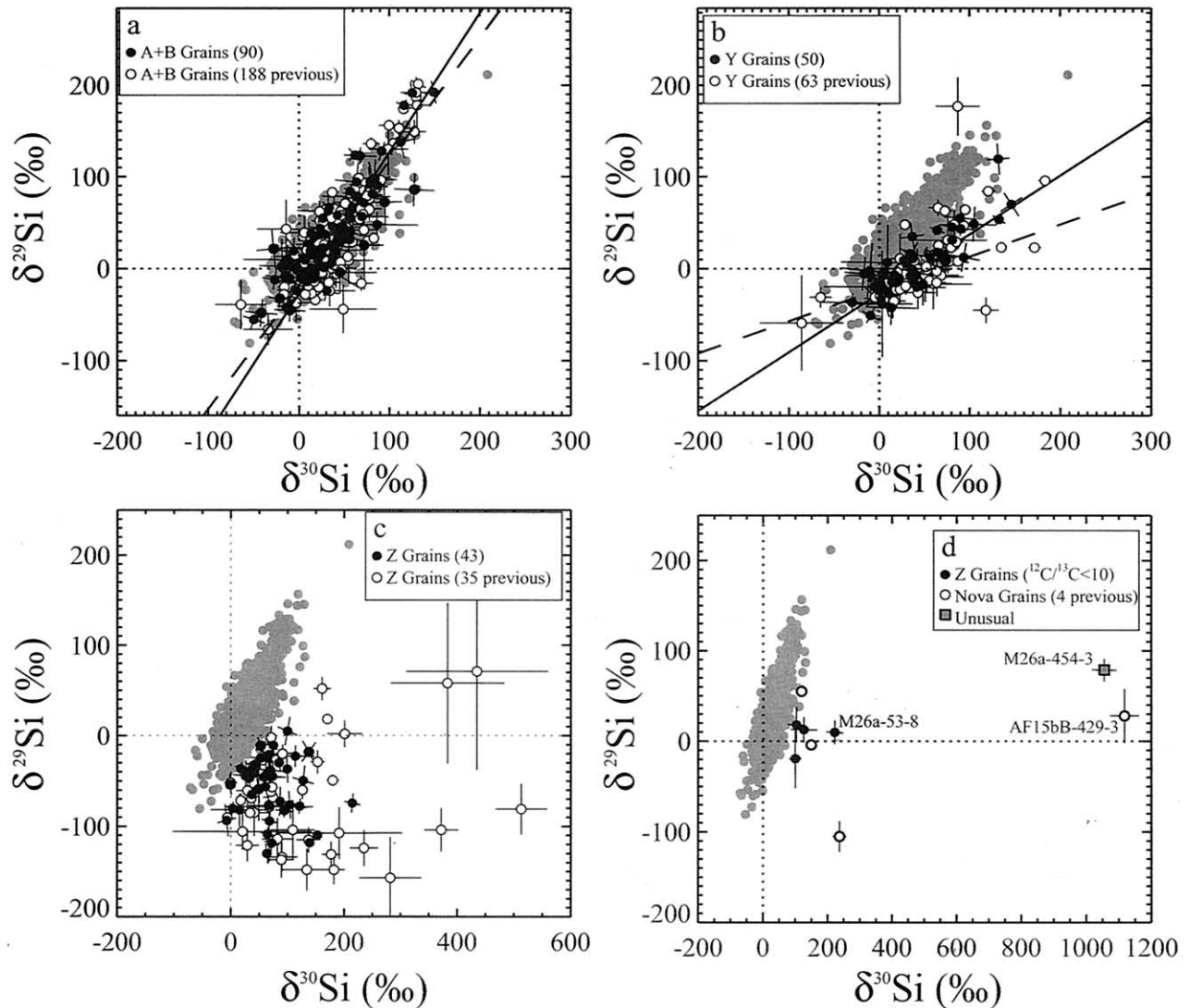
Fig. 13. Silicon δ-values plotted for mainstream SiC from the present study (gray filled symbols) compared with (a) 90 new AB grains and 188 previously reported AB grains (Hoppe et al., 1994; Hoppe et al., 1996a; Amari et al., 2001c). The solid line is a weighted fit to the AB data; it is steeper than the mainstream correlation line indicated by the long dashed line. (b) Fifty new Y grains and 63 previously reported Y grains (Hoppe et al., 1994; Hoppe et al., 1996a; Huss et al., 1997; Amari et al., 2001c). The solid line is a fit to the Y grain data, with a slope intermediate between the original Y-grain line (long-dashes) of Hoppe et al. (1994) and the mainstream correlation line. (c) Forty-three new Z grains with $^{12}C/^{13}C >10$ and 35 previously reported Z grains (Hoppe et al., 1996a; Gao and Nittler, 1997; Hoppe et al., 1997). (d) Four new Z grains with $^{12}C/^{13}C <10$, four previously reported SiC grains with nova C, Si, and N isotopic signatures (Amari et al., 2001a), and ^{30}Si-rich grain M26a-454-3. The new Z grains, especially the ^{30}Si-rich grain M26a-53-8, are strong candidates for having formed in novae. A nova origin is ruled out for M26a-454-3 by its isotopically light C.

good agreement with previous observations and span a very similar range of Si isotopic composition to the mainstream SiC grains. However, a weighted least-squares linear fit to the data for the combined dataset of 280 AB grains (solid line in Fig. 13a) gives a slope of 1.5 ± 0.02, significantly steeper than the slope of 1.35 for the mainstream regression line (long-dashed line in Fig. 13a). Restricting the regression to the 148 grains with errors in Si-isotopic ratios smaller than 10‰ does not change this result. The stellar origins of AB grains are not well understood, as discussed in detail by Amari et al. (2001c). We will not repeat the discussions from that paper here, but we do

note that any ultimate explanation for these grains must account for the subtle difference in Si-isotopic composition.

5.4. Y Grains

Y grains are defined (Table 2, Hoppe et al., 1994; Hoppe and Ott, 1997; Amari et al., 2001b) on the basis of having $^{12}C/^{13}C$ ratios >100, and Si and N isotopic signatures distinct from those of X grains (see below). We identified a total of 50 Y grains, for a total abundance of 1.5%, compared with ~2–4% from previous studies. The lower abundance in our dataset

likely reflects, in part, some background C contamination on sample mounts (see Section 5.1). Si data for the new grains are compared with mainstream SiC and 63 Y grains from previous studies in Figure 13b (^{12}C/^{13}C ratios can be seen in Fig. 9). As for the AB grains, the new Y grains show a similar range of Si isotopic compositions to previous observations. The six Y grains originally identified by Hoppe et al. (1994) plotted on a single line of slope 0.35 on the Si 3-isotope plot (long-dashed line in Fig. 13b) and were considered to have originated in a single parent star. Clearly, a large fraction of the Y grains found subsequently also lie near this line. However, several Y grains lie above this line, and a weighted linear regression to all of the Y grain Si data (solid line in Fig. 13b) gives a slope of 0.64, intermediate between the mainstream correlation line and the original Y-grain line of Hoppe et al. (1994). In any case, as pointed out by previous authors, most Y grains lie to the ^{30}Si-rich side of the mainstream Si-isotopic distribution. The origins of Y grains are discussed in Section 6.

5.5. Z Grains and Nova Grains

SiC grains of type Z, originally identified by Alexander (1993), have ^{29}Si depletions, relative to solar, and ^{30}Si enrichments relative to the mainstream correlation line (Table 2, Hoppe et al., 1997; Hoppe and Ott, 1997). We identified 46 Z grains in our sample, using as our criterion that a Z grain must have δ^{29}Si ≤ 0 and plot more than 2σ to the ^{30}Si-rich side of the mainstream array. Previous studies have shown that the abundance of Z grains in Murchison increases with decreasing grain size. For example, no Z grains were identified among the KJG (3.0-μm) and KJH (4.6-μm) grains studied by Hoppe et al. (1994), but Z grains made up 2.8% of the KJE (1.1-μm) grains of Hoppe et al. (1996a). On the other hand, because Z grains are defined on the basis of Si isotopic ratios, it becomes more difficult to identify them among smaller grains where larger error bars blur the distinction between mainstream and Z grains. Thus it is difficult to compare the abundance found here (1.4%) and the size distribution with previous studies.

Si isotopic ratios for the new Z grains are shown in Figures 13c and 13d, along with mainstream data, and ^{30}Si-rich grains from previous studies. The new Si data overlap the previous observations, but do not reach as extreme compositions (δ^{30}Si > 200‰). However, the most ^{30}Si-rich Z grains from prior studies were identified by direct ion imaging (Gao and Nittler, 1997; Hoppe et al., 1997). This technique is biased towards finding the most extreme grains because the analytical precision is relatively poor, and we therefore think that the difference in range of compositions is a selection effect.

Most previously identified Z grains have ^{12}C/^{13}C ratios comparable to mainstream SiC (20–100), but a handful have lower ratios, down to ~4. The ^{12}C/^{13}C ratios of the new grains show a very similar distribution, ranging from 4 to 80 (Fig. 9). Most Z grains that have been analyzed for N isotopes have ^{14}N/^{15}N ratios higher than the solar value of 272, similar to that observed for mainstream SiC (Hoppe et al., 1997). However, Amari et al. (2001a) reported N data for four SiC grains with Z grain Si isotopic signatures and ^{12}C/^{13}C ratios <10 (Fig. 13d). All four grains were strongly enriched in ^{15}N, (^{14}N/^{15}N = 5–20), and these authors argued that novae (thermonuclear outbursts on the surfaces of white dwarf stars) were the most

likely progenitors of these grains. Nova models do predict very low ^{14}N/^{15}N and ^{12}C/^{13}C ratios, as well as ^{30}Si enrichments relative to ^{29}Si in some cases. In light of the Amari et al. (2001a) data, the four Z grains from the present study with low ^{12}C/^{13}C ratios (Fig. 13d) are strong candidates for also originating in novae, especially grain M26a-53-8, with δ^{30}Si ~200‰. However, confirming such an origin would require additional isotopic evidence, especially N isotopic ratios. The origin of the more abundant Z grains with mainstream-like ^{12}C/^{13}C ratios is discussed in Section 6.

The highly ^{30}Si-enriched grain, M26a-454-3, has a similar Si isotopic composition to that of the grain AF15bB-429-3 from the Acfer 094 meteorite (Fig. 13d, Amari et al., 2001a). Grain AF15bB-429-3 has ^{12}C/^{13}C = 9, arguing for an origin in a nova. In contrast, M26a-454-3 has isotopically light C, with ^{12}C/^{13}C = 118 ± 3 (Fig. 9). Current nova nucleosynthesis models can reproduce fairly well the observed C elemental abundances of nova ejecta (José and Hernanz, 1998) and universally predict very low ^{12}C/^{13}C ratios (Gehrz et al., 1998; José and Hernanz, 1998; Amari et al., 2001a). Thus, a nova source can be ruled out for grain M26a-454-3. On the other hand, it is possible that this grain originated in a supernova. Travaglio et al. (1999) performed mixing calculations of Type II supernova ejecta zones to explain the isotopic compositions of low-density presolar graphite grains. The Si and C composition of M26a454-3 appears to be roughly consistent with some of their mixing calculations (see Figs. 12b and 12c of Travaglio et al., 1999). Isotopic data for additional elements are highly desirable to help confirm or refute a supernova origin for this grain. In any case, the discovery of this grain indicates that we have not yet fully explored the diversity of isotopic compositions of presolar SiC in meteorites.

5.6. X Grains and Si$_3$N$_4$

SiC grains X were originally identified in the Murchison KJG and KJH separates (Amari et al., 1992). They are clearly distinct from other SiC grains in that they are highly enriched in ^{28}Si and ^{15}N, and they typically have isotopically light C and very large ^{26}Mg excesses from decay of (now-extinct) radioactive ^{26}Al originally present at the epoch of grain formation (Hoppe et al., 2000). The isotopic signatures, especially radiogenic ^{44}Ca from 60-year half-life ^{44}Ti, point to an origin in presolar supernova explosions (Nittler et al., 1996; Besmehn and Hoppe, 2003). The rare presolar Si$_3$N$_4$ grains have very similar Si, C, N, and Al-Mg isotopic signatures and thus likely also originated in supernovae (Nittler et al., 1995; Hoppe et al., 1996b). We identified 40 X grains and three presolar Si$_3$N$_4$ grains in our SiC dataset on the basis of having $\delta^{29,30}$Si <–100‰, giving an X grain abundance relative to total SiC of 1.2%. X grains have been found to be present in Murchison at a level of ~1% of total SiC for a wide range of grain sizes (Hoppe et al., 2000), so our abundance estimate is in good agreement with previous data. However, the ratio of Si$_3$N$_4$/SiC-X found here is a factor of ~3 times higher than previously found in Murchison (Nittler et al., 1995), suggesting that Si$_3$N$_4$ survives our chemical procedures better than the standard dissolution methods (see also Section 5.1.).

Si and C isotopic ratios for the new X grains are compared with previous data (Amari et al., 1992; Nittler et al., 1995;
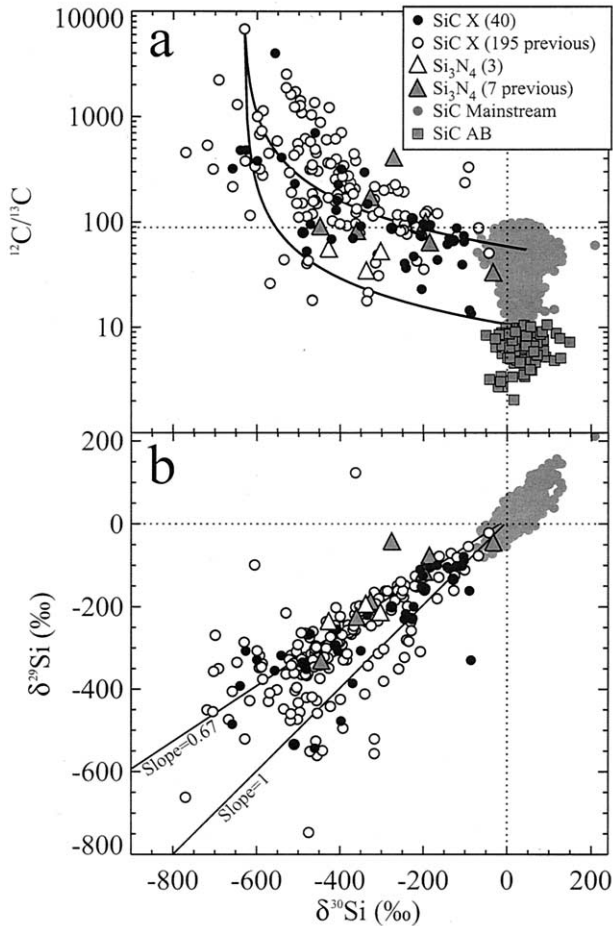
Fig. 14. C and Si isotopic ratios of 40 new X SiC and three new Si$_3$N$_4$ grains compared with data for 195 previously reported X grains (Amari et al., 1992; Nittler et al., 1995; Hoppe et al., 1996a; Nittler et al., 1996; Hoppe et al., 2000) and seven previously reported Si$_3$N$_4$ grains (Nittler et al., 1995; Hoppe et al., 1996a). (a) Carbon-12/carbon-13 is plotted versus δ^{30}Si. The new data show a similar range of compositions to previous data but are, on average, more ^{13}C-rich. Solid curves indicate simple mixing calculations between an extreme X grain composition and a typical mainstream SiC composition (upper curve) and a ^{13}C-rich composition (lower curve). The cluster of new X grains with δ^{30}Si ~ −150‰ and ^{12}C/^{13}C ~ 80 might have included neighboring mainstream grains in their measurements. (b) δ^{29}Si plotted versus δ^{30}Si. The new data span a similar range of Si isotopic composition to previous observations, with most grains lying close to a line of slope 0.67. One grain plots significantly to the ^{30}Si-rich side of all the previous data.

Hoppe et al., 1996b; Nittler et al., 1996; Hoppe et al., 2000) for SiC X and Si$_3$N$_4$ grains in Figure 14. The new grains show a similar range of silicon isotopic ratios to the prior data (Fig. 14b). The majority of grains lie along a line of slope 0.67 (Nittler et al., 1995), though several grains plot significantly away from this line, mostly towards the slope-1 mixing line connecting pure ^{28}Si with the solar composition. One new grain plots significantly to the right of all previous data, at a composition of δ^{29}Si ~ −320‰, δ^{30}Si ~ −100‰.

Carbon isotopes are plotted in Figure 14a. The new data span a similar range of ^{12}C/^{13}C ratios to the older data, from ~10 to ~4000. However, the C-isotopic distribution of the present

work is skewed towards lower ratios. The median ^{12}C/^{13}C ratio of the new grains is 91, compared with the value of 185 found for the previous data. Moreover, 62% (25/40) of the new X grains have ^{12}C/^{13}C <100, compared to 28% of the previous data (Hoppe et al., 2000). The problems of contamination and grain aggregation discussed previously in Section 5.1 probably play a role in explaining this discrepancy. Carbon-13 rich background (either from contamination or from neighboring mainstream SiC grains) will disproportionally affect measurements of grains with very high ^{12}C/^{13}C ratios. Terrestrial C contamination can explain the relative lack of grains in our sample with ^{12}C/^{13}C >500, but cannot explain the higher abundance of ^{13}C-rich X grains.

To investigate the possibility of grain aggregation as an explanation for the ^{13}C-richness of our grains, we performed simple mixing calculations. The upper curve in Figure 14a indicates the compositions expected for isotopic mixtures of the most ^{13}C-poor X grain with the average composition of mainstream SiC. The lower curve indicates mixtures of the same extreme X grain composition with a very ^{13}C-rich composition (^{12}C/^{13}C = 10). Several of the new X grains lie along the mixing curve with the mainstream average. The cluster of five grains with δ^{30}Si ~ −150‰, ^{12}C/^{13}C ~60 would require up to 35% of their measured Si and C ions to have come from neighboring mainstream SiC grains to explain their compositions. The other ^{13}C-rich grains would require the statistically less likely scenario of mixing with grains with atypically low ^{12}C/^{13}C ratios, in some cases down to 10 (lower mixing curve). In any case, if we generously assume that 10 of the new ^{13}C-rich X grains actually have true ^{12}C/^{13}C ratios >100, the relative abundance of ^{13}C-rich grains drops to 37% of the total X grains. This is still higher than previously observed, suggesting that a population of ^{13}C-rich X grains preferentially survives our chemical treatments, but the statistical significance of this result is not very high. For example, if we assume that the "true" abundance of ^{13}C-rich X grains is 30%, then a binomial distribution predicts that the probability of finding ≥15 ^{13}C-rich grains out of 40 grains is 20%.

Silicon nitride is more susceptible to C contamination than SiC, and all three presolar Si$_3$N$_4$ grains of the present study have ^{12}C/^{13}C ratios lower than solar. SEM examination indicates that C contribution from a nearby SiC grain was likely for one of the three grains, but not for the others. For the two "clean" grains, measured Si/C ratios were in the range previously observed for presolar Si$_3$N$_4$ (Nittler et al., 1995), further arguing that their C is intrinsic. The majority of previously observed Si$_3$N$_4$ grains also have isotopically heavy C.

6. SiC MAINSTREAM, Y, AND Z GRAINS: ORIGINS AND IMPLICATIONS

6.1. Asymptotic Giant Branch Stars and SiC Grains

Together, the mainstream, Y, and Z subgroups make up >95% of presolar SiC in meteorites. Carbon-rich asymptotic giant branch (AGB) stars have been proposed as the progenitors of all three grains groups (Hoppe et al., 1997; Hoppe and Ott, 1997; Amari et al., 2001b). The AGB phase of stellar evolution follows core He-burning in low-mass and intermediate-mass (M = 1–8M$_\odot$) stars (Iben and Renzini, 1983; Straniero et al., 1997; Busso et al., 1999). AGB stars consist of an

inert C-O white dwarf core surrounded by thin shells of He, H and a very large convective H-rich envelope. At the beginning of the AGB phase, the envelope composition has been already slightly modified by convective mixing (so-called first, and in stars more massive than ~3M$_\odot$, second dredge-ups) of material partially processed by core and shell H burning. Periodic thermal pulses occur during the AGB phase, in which nuclear burning alternately occurs in the He and H shells. Material modified by the shell burning is convectively mixed into the stellar envelope in a recurrent process known as the third dredge-up. This material is strongly enriched in ^{12}C and in nuclei produced by the s-process (slow neutron capture) nucleosynthesis. Thus, a major result of the third dredge-up is to enrich the stellar surface in ^{12}C, gradually increasing the C/O and ^{12}C/^{13}C ratios. When the C/O ratio approaches unity, the chemistry of the envelope fundamentally changes and the star becomes a carbon star. The C/O ratio must exceed unity in order for phases like SiC to form, since at lower ratios most of the C is locked up in the very stable CO molecule. See Busso et al. (1999) for a recent review of nucleosynthesis in AGB stars.

Beyond shell burning and third dredge-up, two additional nucleosynthesis processes are expected to occur in some AGB stars: cool bottom processing (CBP) and hot bottom burning (HBB). In stars of ≤2.3M$_\odot$, cool bottom processing may mix material from the base of the convective envelope to deeper, hotter layers (where its composition is modified by nuclear reactions) and back again (Charbonnel, 1995; Wasserburg et al., 1995; Denissenkov and Weiss, 1996; Boothroyd and Sackmann, 1999; Nollett et al., 2003). The physical mechanism behind CBP has not been identified, but there is substantial observational evidence, from stars and from presolar grains, that it occurs in stars on both the red giant and asymptotic giant branches (Charbonnel, 1995; Huss et al., 1997; Boothroyd and Sackmann, 1999; Nollett et al., 2003). In stars >~4M$_\odot$, the base of the convective envelope becomes hot enough for H-burning reactions to directly change the envelope composition (HBB, Cameron and Fowler, 1971; Boothroyd et al., 1995). Both CBP and HBB have the effect of directly modifying the envelope composition, in particular decreasing C/O and ^{12}C/^{13}C ratios and thus preventing or delaying C-star formation.

A very large body of evidence now supports an AGB star origin for the mainstream SiC grains (Hoppe et al., 1994; Hoppe and Ott, 1997; Lugaro et al., 1999). Among the supporting arguments are: 1) the distribution of ^{12}C/^{13}C ratios (Fig. 8) of the mainstream SiC matches closely the distribution measured spectroscopically in C stars (Smith and Lambert, 1990); 2) an infrared feature attributable to solid SiC is commonly observed around C stars (Speck et al., 1997); 3) the isotopic compositions of many trace elements show enrichments in s-process isotopes, both for elements measured in aggregates of many grains (Sr, Ba, Nd, Sm, Dy, and noble gases, reviewed by Hoppe and Ott, 1997) and, more recently, for elements analyzed by resonance ionization mass spectrometry in single grains (Sr, Zr, Mo, and Ba, Nicolussi et al., 1997; Nicolussi et al., 1998a; Nicolussi et al., 1998b; Savina et al., 2003). In fact, most isotopic signatures measured in mainstream SiC grains are generally in very good quantitative agreement with those predicted by numerical models of AGB stars (Lugaro et al., 2003). Finally, 4) C-stars are the dominant

stellar source of carbonaceous dust in the interstellar medium (Whittet, 2002).

A significant exception to the match between mainstream SiC isotopic compositions and those observed or predicted for AGB stars concerns the 50% of the grains' atoms that are Si. Neutron capture reactions are expected to slightly increase ^{29}Si/^{28}Si and ^{30}Si/^{28}Si ratios in the AGB He shell, but the models predict larger effects for ^{30}Si than for ^{29}Si. This corresponds to evolution in a Si δ-value plot along lines of slope <1 (~0.3–0.7 for recent models), in sharp contrast to the slope 1.35 line observed for mainstream SiC (Fig. 11). Moreover, at least for stars with similar chemical compositions to the Sun, once the He-shell material is diluted by mixing with the envelope during the third dredge-up, the predicted change in Si isotopic composition (Lugaro et al., 1999) is much smaller than the observed range in SiC (20‰ predicted vs. the observed ~200‰). It is now accepted that the mainstream SiC array largely reflects a wide range of initial Si isotopic compositions of the parent stars, with only minor modifications from nucleosynthesis within the stars themselves (Alexander, 1993). A similar case has been made for Ti: the Ti isotopic ratios correlate with Si isotopic ratios in mainstream SiC, though the ^{49}Ti/^{48}Ti and ^{50}Ti/^{48}Ti ratios seem to also have a significant neutron capture component from the parent AGB stars (Hoppe et al., 1994; Alexander and Nittler, 1999).

The most common explanation for the range of Si and Ti isotopic compositions is the chemical evolution of the Galaxy (GCE): as new generations of stars are born, live their lives, and expel newly synthesized material into the interstellar medium, the elemental and isotopic composition of the galaxy changes. A key parameter of GCE studies is the metallicity (Z), the mass fraction of elements heavier than He in a particular astrophysical environment (Z$_\odot$ = 2%). Because the nucleosynthetic yields of different isotopes from different stars often depend on the metallicity, mean isotopic ratios of the interstellar medium (and hence new stars) are expected to change with time (Clayton, 1988). For example, Timmes and Clayton (1996) calculated the expected GCE of Si isotopes and predicted that the mean composition of the galaxy should evolve along a line of slope 1 on a Si δ-value plot, with lower metallicity stars having lower ^{29,30}Si/^{28}Si ratios. Alternatively, Lugaro et al. (1999) interpreted the mainstream SiC Si isotope array as arising from a combination of GCE and inhomogeneous mixing of supernova ejecta into different regions of the interstellar medium. This model fails to explain the high degree of correlation observed between Si and Ti isotopic ratios, however (Nittler, 2002).

As originally pointed out by Hoppe et al. (1994), the SiC Y grains also have isotopic signatures pointing to an origin in AGB stars. The higher ^{12}C/^{13}C ratios and ^{30}Si/^{29}Si ratios, compared with mainstream SiC, indicate a higher fraction of He-shell material in the envelopes of the Y grain parent stars, however. Amari et al. (2001b) reported C, N, Si, Mg-Al, and Ti isotopic data for 27 SiC Y grains identified by direct ion imaging. They argued that the most likely stellar sources of Y grains were AGB stars of somewhat lower than solar metallicity. As metallicity decreases, the effect of the third dredge-up on the surface composition of AGB stars dramatically increases, due to the smaller dilution of He-shell material with the initially heavy-element depleted envelope. Detailed compari-
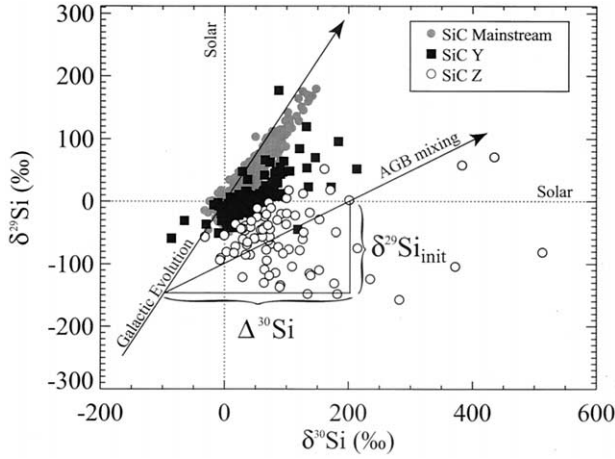
Fig. 15. Si isotopic ratios for mainstream, Y, and Z presolar SiC grains from this and previous studies (see Figs. 8 and 13 for references). All three grain groups are believed to originate in C-rich asymptotic giant branch stars. The Si isotopic composition of any individual grain can be deconvolved into the initial composition of its parent star, assumed to lie along the Galactic evolution line and the composition due to mixing during the AGB phase, assumed to evolve along a mixing line of slope 0.5. As illustrated, $\delta^{29}Si_{init}$ is a measure of the grain progenitor initial composition and $\Delta^{30}Si$ is a measure for the amount of AGB mixing.

son of C, Si, and Ti isotopic compositions of the Y grains with AGB models of different masses and metallicities indicated good agreement for stars of $\sim 1/2\ Z_\odot$ and a range of stellar masses ($> 1.5 M_\odot$, possibly up to $5 M_\odot$). These authors also showed that, when a theoretical n-capture component is subtracted from the Y grains' Si isotopic ratios, the inferred initial $^{29,30}Si/^{28}Si$ ratios are typically lower than those of mainstream grains, as expected from GCE models for lower than solar metallicity stars.

SiC Z grains typically show even larger ^{30}Si excesses relative to mainstream grains than do the Y grains, though their $^{12}C/^{13}C$, $^{14}N/^{15}N$ and inferred $^{26}Al/^{27}Al$ ratios are similar to those of mainstream grains. Hoppe et al. (1997) suggested that the most likely origin of these grains was in AGB stars of even lower metallicity, $Z \sim Z_\odot/3$. These authors further argued that the lower $^{12}C/^{13}C$ ratios of Z grains, relative to the Y grains, requires that extensive cool bottom processing occurred in the parent stars before the AGB phase and perhaps during the AGB as well.

6.2. Silicon Isotopic Trends in Mainstream, Y, and Z SiC Grains

For the most part, previous studies have considered the mainstream, Y, and Z grains independently. With the significantly larger isotopic database presented here, we are now in a position to explore the relationships between these groups in more detail. For example, the separate studies described above discuss three distinct metallicity regimes: $Z = Z_\odot$, $Z_\odot/2$, and $Z_\odot/3$ for mainstream, Y, and Z grains, respectively, yet a key question is whether or not the groups represent a smooth sequence over this large metallicity range. The Si isotopic ratios for the three SiC groups are shown again in Figure 15; for

clarity, error bars are omitted and only the highest precision mainstream data are included (Si errors $<10\permil$). Based on the foregoing discussions, the Si isotopic composition of any single grain is the sum of two components. One, the initial composition of the parent star, is assumed to lie along a line representing the mean chemical evolution of the Galaxy ("Galactic Evolution" line). The second component is due to the mixing of He-shell material into the stellar envelope by third dredge-up ("AGB Mixing" line). Following previous work (Hoppe et al., 1997; Amari et al., 2001b), we have projected the Si isotope data for each grain onto the Galactic evolution (GCE) line, along an assumed AGB mixing line. This procedure is essentially a nonlinear coordinate transformation that converts the original $\delta^{30}Si$, $\delta^{29}Si$ values into new quantities labeled $\delta^{29}Si_{init}$ and $\Delta^{30}Si$, as illustrated in Figure 15. The resulting $\delta^{29}Si_{init}$ values are the inferred starting compositions of the grain parent stars and hence proxies for metallicity, whereas the $\Delta^{30}Si$ values are a measure of the amount of He-shell material dredged-up to the stellar envelopes. This procedure depends on the assumed slopes of the Galactic evolution and AGB mixing lines, and the results should thus be taken as illustrative of trends, not as quantitatively rigorous. Here, we assumed that the Si isotopic composition of the Galaxy evolves along a line of slope 1.5, passing through solar, based on the GCE model of Alexander and Nittler (1999). We also assumed that the slope of the AGB mixing line is always 0.5. However, AGB models in fact indicate a range of slopes from 0.4 to 0.7 for stars of different masses and metallicities (Lugaro et al., 1999). Error bars on $\delta^{29}Si_{init}$ and $\Delta^{30}Si$ values were generated by propagating both the measurement errors and an assumed error of ± 0.2 in the AGB mixing line slope.

The inferred $\Delta^{30}Si$ and $\delta^{29}Si_{init}$ values are plotted in Figure 16 for the mainstream, Y, and Z SiC grains. For $\delta^{29}Si_{init} > 0$ (primarily mainstream grains), the trend is basically flat, but there is a remarkably smooth linear trend between the two quantities for $\delta^{29}Si_{init} < 0$. The relationship is clearest for the Z grains, because they span a much wider range of $\delta^{29}Si_{init}$ values than the Y grains do, but the Y grains do appear to also follow the trend. The smooth trend from Z to Y to mainstream suggests that the grain groups are related in the sense that they probably formed from stars with an approximate continuum of metallicities as opposed to a set of a few discrete compositions.

Qualitatively, Figure 16 is consistent with predictions that lower metallicity AGB stars are more strongly affected by third dredge-up. For example, the maximum $\Delta^{30}Si$ values predicted for low-mass AGB stars are $\sim 35\permil$, $\sim 200\permil$, and $\sim 400\permil$ for metallicities of solar, one-half solar, and one-third solar, respectively (Hoppe et al., 1997; Lugaro et al., 1999; Amari et al., 2001b). However, the results shown in Figure 16 raise some interesting questions. First, comparing the $\Delta^{30}Si$ predictions to the values inferred for the grains suggests that $Z = Z_\odot/2$ corresponds to $\delta^{29}Si_{init} \sim -150\permil$ and $Z = Z_\odot/3$ to $\delta^{29}Si_{init} \sim -300\permil$. With $\delta^{29}Si_{init} = 0$ for solar metallicity, these results suggest that the $\delta^{29}Si_{init}$–Z relationship is strongly nonlinear, in contrast to expectations from Galactic chemical evolution models (Timmes and Clayton, 1996). This was previously pointed out by Amari et al. (2001b) and, as discussed by these authors, has potentially important implications for the relative rates of Type Ia versus Type II supernova explosions in the Galaxy. Second, the AGB models predict that the third dredge-up
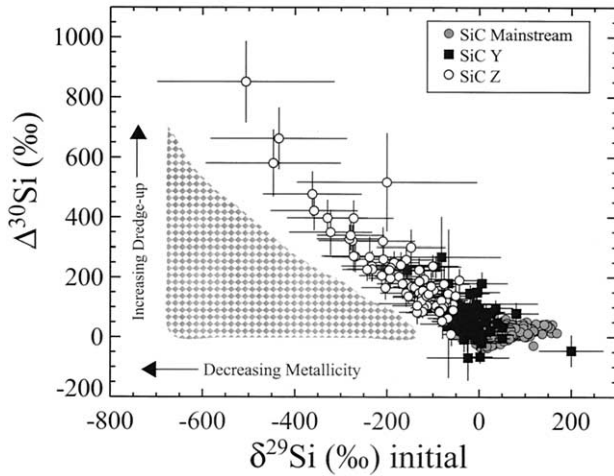
Fig. 16. Inferred $\Delta^{30}Si$ values plotted against $\delta^{29}Si_{init}$ values for mainstream, Y, and Z SiC grains (see text and Fig. 15 for definitions of plotted quantities). For $\delta^{29}Si_{init} > 0$, the trend is flat, indicating minor third dredge-up of Si isotopes in AGB stars of close-to-solar metallicity. Below $\delta^{29}Si_{init} = 0$, the grains plot along a smooth linear trend, consistent with AGB star models that predict $\Delta^{30}Si$ to increase with decreasing metallicity (Amari et al., 2001b). In contrast to expectations, no grains with very low $\delta^{29}Si_{init}$ also have low $\Delta^{30}Si$ values (stippled triangular region), possibly indicating strong cool bottom processing in early thermal pulses in low-metallicity AGB stars.

substantially increases the surface ^{12}C abundance before significantly modifying the Si isotopic ratios. Even for very low metallicity stars, $\Delta^{30}Si$ values are expected to be relatively small when the star becomes C-rich and only increase after many additional thermal pulses. Thus, in low-metallicity AGB stars, SiC grains could be expected to form with a range of $\Delta^{30}Si$ values from a few tens of permil up to several hundred permil. This is apparent for the Y grains in Figure 16, but there are no Z grains with very low values of both $\delta^{29}Si_{init}$ and $\Delta^{30}Si$ (stippled triangular region in Fig. 16). One possible explanation is that SiC only forms after many thermal pulses, because mass-loss rates increase with time during the AGB phase and grain formation efficiency is higher at higher mass-loss rates. Alternatively, cool bottom processing (CBP) or hot bottom burning (HBB) may play a role; to understand why, we now turn to the C isotopes.

6.3. Silicon and Carbon Isotopes in Mainstream, Y, and Z SiC Grains

Shown in Figure 17 are the inferred $\Delta^{30}Si$ and $\delta^{29}Si_{init}$ values plotted against $^{12}C/^{13}C$ ratios for the mainstream, Y, and Z grains. Also plotted in Figure 17a are model AGB $\Delta^{30}Si$-$^{12}C/^{13}C$ trajectories. Thick dashed curves are predictions for AGB stars with metallicity $Z = Z_\odot/2$ and masses $3M_\odot$ and $5M_\odot$ from Amari et al. (2001b). The trajectory for $1.5M_\odot$ stars of this metallicity follows closely the $3M_\odot$ curve, but only reaches a $^{12}C/^{13}C$ ratio of ~200. As discussed by Amari et al. (2001b), these models bracket most of the Y grain data and thus suggest that these grains formed in stars of approximately half-solar metallicity and masses in the range 1.5–5 $M_\odot$. The thick solid curves in Figure 17a are predictions (Hoppe et al., 1997; Amari et al., 2001b) for $3M_\odot$ AGB stars with $Z = Z_\odot/3$ and three
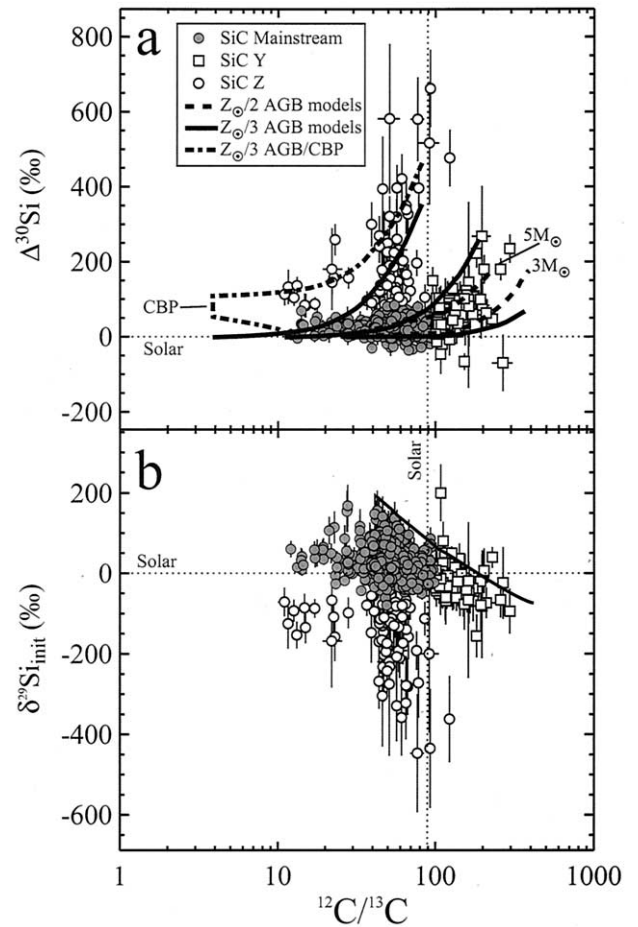

Fig. 17. $\Delta^{30}Si$ and $\delta^{29}Si_{init}$ values plotted against $^{12}C/^{13}C$ ratios for mainstream, Y, and Z SiC grains. (a) $\Delta^{30}Si$ values plotted against $^{12}C/^{13}C$ ratios for mainstream, Y, and Z SiC grains. Predictions for low-metallicity AGB star envelopes are indicated by thick curves. Dashed curves indicate $Z_\odot/2$ models with the indicated masses. Y grain compositions are bracketed by these models, suggesting an origin in AGB stars with $Z \sim Z_\odot/2$ and a range of masses up to $5M_\odot$. Solid curves indicate models for $3M_\odot$ stars with even lower metallicity ($Z_\odot/3$) and three assumed initial $^{12}C/^{13}C$ ratios: 3.5 (upper), 10 (middle), and 24 (lower). Z grain compositions are roughly consistent with the model with initial $^{12}C/^{13}C = 3.5$, but many grains plot to the ^{30}Si-rich side of this curve. The dashed-dot curve shows schematically the effect that either strong cool bottom processing or hot-bottom burning in early thermal pulses would have on the low-metallicity $\Delta^{30}Si$-$^{12}C/^{13}C$ curve. (b) $\delta^{29}Si_{init}$ values plotted against $^{12}C/^{13}C$ ratios for mainstream, Y, and Z SiC grains. There is an apparent sharp threshold of $\delta^{29}Si_{init} \sim -80‰$ below which few grains have $^{12}C/^{13}C > 70$. Above this value, the maximum observed $^{12}C/^{13}C$ ratio decreases as $\delta^{29}Si_{init}$ increases (solid curve), suggesting that both the effectiveness of third dredge-up and the typical mass of the SiC parent stars decrease with increasing metallicity.

assumed initial $^{12}C/^{13}C$ ratios at the start of the AGB phase: 3.5 (upper curve), 10 (middle), and 24 (lower). Clearly, the $\Delta^{30}Si$–$^{12}C/^{13}C$ trajectories depend strongly on the starting $^{12}C/^{13}C$ ratio. A value of 24 is typical for first dredge-up in red giants more massive than ~2.3 $M_\odot$. Lower values would require that the star experienced CBP before the AGB and thus was less massive than ~2.3$M_\odot$ (Boothroyd and Sackmann, 1999). Thus, there is some inconsistency in assuming low pre-AGB $^{12}C/^{13}C$

values for a 3M$_\odot$ AGB star, as was done by Hoppe et al. (1997), but it at least allows a qualitative comparison with the data.

Of the Z$_\odot$/3 curves in Figure 17a, only the uppermost (initial ^{12}C/^{13}C ratio of 3.5) approaches consistency with the Z grain data. However, as previously pointed out by Hoppe et al. (1997), many of the Z grains still lie to the high Δ^{30}Si side of this curve. These authors suggested that this might be explained either if the early thermal pulses have higher ^{30}Si/^{28}Si ratios than predicted or if some CBP occurs during the AGB phase (not included in the models). The thick dot-dashed curve in Figure 17a indicates schematically the effect of strong CBP during early thermal pulses. This star is assumed to begin the AGB phase with a ^{12}C/^{13}C ratio of 10, reflecting some CBP during the red giant phase of evolution. Extensive CBP rapidly decreases this ratio to the nuclear equilibrium value of 3.5 for several thermal pulses. Because Si isotopes are not affected by CBP, the third dredge-up gradually increases the ^{30}Si/^{28}Si ratio during these pulses. Once CBP ceases (at a Δ^{30}Si value of 100‰ in this schematic example), third dredge-up rapidly increases the ^{12}C/^{13}C ratio while continuing to gradually increase Δ^{30}Si. Clearly, such a model could provide a better fit to the Z grain data, but needs to be confirmed by numerical calculations. One attraction of this scenario is that the C/O ratio remains low during the extensive CBP, precluding SiC formation until the CBP drops off. This provides a natural explanation for the missing data in Figure 16 (triangular region), because SiC grains would not be expected to form with low Δ^{30}Si values. Calculations by Boothroyd and Sackmann (1999) suggest that the strength of CBP in AGB stars should increase roughly as Z^{-1}. This would then suggest that the minimum Δ^{30}Si value observed in SiC grains should increase with decreasing metallicity, in general agreement with the Z grain trend in Figure 16.

We note that, although this discussion has assumed that CBP is the operative process, all that is needed is for the stellar envelope to be strongly processed by CNO-burning during early thermal pulses. Thus, hot bottom burning in an intermediate-mass (M $\sim4-8$M$_\odot$) AGB star could qualitatively result in the same trend illustrated by the dash-dot curve in Figure 17a. In this case, the initial AGB ^{12}C/^{13}C ratio would be higher, in the range of 20–30, but would still be rapidly decreased to the equilibrium value of $\sim$3.5. The large Δ^{30}Si values of the Z grains are certainly consistent with an origin in intermediate-mass AGB stars, since more massive stars are predicted to have larger shifts in their Si isotopic ratios (Fig. 17a). Moreover, HBB requires a minimum envelope mass to occur. Calculations by Frost et al. (1998) of low-metallicity intermediate-mass AGB stars indicate that mass loss can lead to cessation of HBB while third dredge-up continues, leading ultimately to formation of C-stars. Thus, the requirement that the CNO-processing ceases after some number of thermal pulses to explain the Z grain data is easily explained in a HBB scenario. One difficulty with this scenario is that the final ^{12}C/^{13}C ratio never exceeds 15 in the HBB models of Frost et al. (1998), but the number of cases considered was small. In summary, much of the Z grain data seems to require CNO-processing of the AGB envelope itself, indicating either CBP in low-mass stars or HBB in intermediate-mass stars. Unfortunately, the present data are not sufficient to unambiguously determine between these possibilities. Isotopic measurements of trace elements (e.g., Ba) in
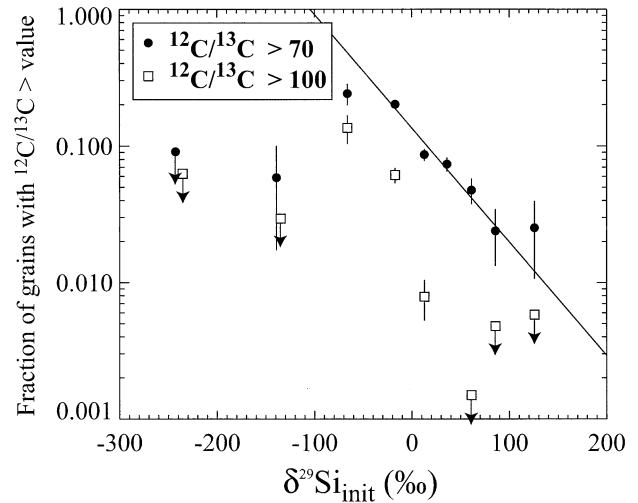

Fig. 18. The fraction of grains with ^{12}C/^{13}C > 70 and 100 as a function of δ^{29}Si$_{init}$ for presolar SiC grains of type mainstream, Y, and Z. Upper limits are given for δ^{29}Si$_{init}$ bins containing no grains with high ^{12}C/^{13}C ratios. Y grains span a very narrow range of initial Si isotopic composition. Above δ^{29}Si$_{init}$ $\sim$ 0‰, the abundance of grains with ^{12}C/^{13}C > 70 decreases exponentially with increasing δ^{29}Si$_{init}$ (solid line).

single Z grains could be diagnostic, however, because the He-shell isotopic composition is strongly mass-dependent (Lugaro et al., 2003).

Unlike in Figure 16, where the Z, Y, and mainstream SiC grains form a single smooth distribution, the Y and Z grains are clearly distinct in both panels of Figure 17. In fact, the Y and Z grains appear to represent the extreme ends of two distinct trends that merge independently into the mainstream data. A striking feature of Figure 17b is that there appears to be a threshold value of δ^{29}Si$_{init}$ $\sim$ -80‰, immediately above which the mainstream and Y grains form a continuous distribution with ^{12}C/^{13}C = $\sim$30 –$\sim$300 and below which almost all grains have ^{12}C/^{13}C < $\sim$70. Furthermore, as δ^{29}Si$_{init}$ increases from this threshold, the maximum observed ^{12}C/^{13}C value decreases, so that the data are roughly bounded on the upper right by a diagonal line (solid curve in Fig. 17b). Huss et al. (1997) noted this trend for the mainstream grains and argued that it reflected the increasing effect of third dredge-up on the AGB envelope ^{12}C/^{13}C ratio with decreasing metallicity.

With the large database reported here, we can investigate the trends of Figure 17b in more detail. We have divided the data into several δ^{29}Si$_{init}$ bins and counted the number of grains with ^{12}C/^{13}C ratios higher than 70 and 100 in each bin. To avoid biasing the data, we have excluded Y and Z grains identified by direct ion imaging techniques (Hoppe et al., 1997; Amari et al., 2001b). Results are shown in Figure 18. Grains with ^{12}C/^{13}C > 100 (Y grains) are only present for a narrow range of initial Si compositions (δ^{29}Si$_{init}$ = -80‰ to $\sim$0‰), but make up $\sim$10% of grains in this range. The fraction of grains with ^{12}C/^{13}C > 70 is small for very low δ^{29}Si$_{init}$ values, but jumps to $\sim$25% of the total grains with δ^{29}Si$_{init}$ $\sim$ -80‰. Above this value, the fraction falls steeply with increasing δ^{29}Si$_{init}$, such that grains with high ^{12}C/^{13}C ratios make up only $\sim$1–2% of the total with δ^{29}Si$_{init}$ > +80‰. The fact that the

$^{12}C/^{13}C > 70$ fraction for the highest bins plot along a straight line on this semilog plot (solid line) indicates that the falloff in abundance above $\delta^{29}Si_{init} > 0$ is approximately exponential.

As discussed earlier, the Si trend shown in Figure 16 provides evidence for either strong CBP or HBB to occur in the early thermal pulses of the low-metallicity AGB parent stars. In this context, the value of $\delta^{29}Si_{init} = -80‰$ probably corresponds to a metallicity threshold below which the relevant process (CBP or HBB) in AGB stars is stronger and more common than at higher metallicity. If the Z grains originated in low-metallicity stars experiencing CBP, the relatively abrupt change in behavior certainly carries important information about the still not understood physical mechanism for CBP. If they are instead from more massive stars in which HBB occurred, the cutoff might indicate a threshold above which HBB never ceases and C-stars do not form.

The trend in Figure 18 is qualitatively consistent with the simple expectation that AGB stars of lower metallicity can reach higher $^{12}C/^{13}C$ ratios than can higher metallicity stars (Huss et al., 1997). The AGB He-shell ^{12}C abundance is independent of metallicity, but the initial envelope abundance is directly proportional to Z. For the same initial $^{12}C/^{13}C$ ratio and the same amount of He-shell material mixed to the surface during the third dredge-up, the expected envelope $^{12}C/^{13}C$ ratio is proportional to $1/Z$. The observed exponential relationship between the fraction of mainstream and Y SiC grains with high $^{12}C/^{13}C$ ratios and the inferred $\delta^{29}Si_{init}$ values would thus seem to provide further evidence that the relationship between $^{29}Si/^{28}Si$ and metallicity is highly nonlinear, as discussed above and by Amari et al. (2001b). However, the expected AGB $^{12}C/^{13}C$ ratio depends not only on metallicity, but also increases with increasing stellar mass (Amari et al., 2001b). Lugaro et al. (1999, 2003) have presented several lines of evidence that most mainstream SiC grains originated in AGB stars less massive than 3 $M_\odot$. In contrast, taking the $Z = Z_\odot/2$ AGB models at face value, a significant fraction of the Y grains must have originated in stars between 3 and 5$M_\odot$ (Fig. 17a and Amari et al., 2001b). Thus, the trend for $\delta^{29}Si_{init} > -80‰$ seen in Figure 18 appears to indicate a strong and systematic increase in the maximum mass of SiC progenitor AGB stars with decreasing metallicity. This result is surprising: because the average metallicity of the Galaxy increases with time and less massive stars live longer than more massive ones, we would expect to see the opposite trend to what is observed. That is, low-mass parent stars would be expected to have been formed earlier and have lower metallicity, on average, than more massive ones. If the Z grains actually originated in stars more massive than 4$M_\odot$, as discussed previously, the surprising trend is extended to very low metallicities.

The empirical trends evident in Figures 16–18 clearly contain a wealth of information about nucleosynthesis and mixing processes in AGB stars as a function of metallicity as well as the distribution of masses and metallicities of stars that provided SiC to the early Solar System. However, any realistic quantitative interpretation of the isotopic data will require a much more extensive set of AGB star models of different masses and metallicities and including cool bottom processing. Moreover, isotopic data for additional elements in a larger number of grains are highly desirable. For example, heavy trace elements measured by resonance ionization mass spectrometry

(Nicolussi et al., 1997; Lugaro et al., 2003) can be quite diagnostic of the mass and metallicity of the parent stars, but such data are very sparse for both Y and Z grains.

7. CONCLUSIONS

We have described a new analytical system developed to enable fully automated location and isotopic analysis of micron-sized particles using secondary ion mass spectrometry. Tests on terrestrial standards confirm that the system can measure Si, C, and O isotopic ratios in particles with the same accuracy and precision as traditional manual grain analyses. Although the data are not shown here, we have also obtained S and Mg isotopic data from standards with similar results. Several hundred particles can be analyzed per day. This is less efficient than the method of direct SIMS imaging (Nittler et al., 1997; Simons et al., 1998; Hoppe et al., 2000), but the attainable measurement precision is much higher with the new system. Moreover, it can be used to measure isotopic ratios, such as $^{17}O/^{16}O$, that are not measurable using direct ion imaging.

As an initial application of the particle measurement system, we have obtained Si and C isotopic ratios for more than 3300 presolar SiC grains of size 0.5–4 μm, extracted from the Murchison CM2 meteorite. Three rare presolar Si_3N_4 grains were identified as well. This more than triples the available database of both C and Si isotopes in presolar SiC. In addition to members of the known subgroups of presolar SiC, a highly unusual grain with an extreme ^{30}Si enrichment, a modest ^{29}Si enrichment and isotopically light C was identified. The new SiC data are broadly consistent with previous studies of SiC in both Murchison and other primitive meteorites. Minor differences in isotopic distributions between the new and previous data are probably due, in part, to problems of background contamination and grain aggregation on sample mounts. These problems are not a weakness of the mapping system itself, but indicate the importance of preparing sample mounts with well-dispersed grains. Future studies will also include routine automated scanning electron microscope characterization of sample mounts to monitor potential problems of grain aggregation. It is likely that some of the differences between old and new SiC data are intrinsic to the samples, reflecting the fact that a new and less harsh chemical procedure was used here to extract the SiC grains.

Three groups of SiC grains—mainstream, Y, and Z—are believed to have originated in AGB stars with a range of initial compositions (metallicity). We have used the large database of presolar SiC obtained here together with previous data to explore the relationships between these three groups of grains. Although the Si isotopic ratios of Z, Y, and mainstream grains are consistent with their representing a smooth trend from very low to approximately solar metallicities, the C isotopic ratios indicate that the Y and Z grains merge into the mainstream trend independently. Comparison with AGB star models indicates that the parent stars of the Z grains most likely experienced either strong CBP or HBB during the AGB phase, whereas the Y and mainstream grains did not. A HBB explanation for the Z grain data would require that the grains originated in intermediate-mass ($M > 4M_\odot$) stars, in conflict with previous suggestions (Hoppe et al., 1997) but consistent with the available isotopic data. The Si and C isotopic data

suggest a sharp metallicity cutoff below which either CBP or HBB occurs during the AGB phase. The fraction of mainstream and Y SiC grains with $^{12}C/^{13}C$ ratios higher than 70 decreases exponentially with increasing initial $^{29}Si/^{28}Si$ ratio. This is consistent with the expectation that lower metallicity stars have higher $^{12}C/^{13}C$ ratios than higher metallicity ones, though the trend suggests a highly nonlinear relationship between initial Si isotopic composition and metallicity. Surprisingly, the data also seem to require that the maximum mass of grain parent AGB stars increases sharply with decreasing metallicity, in contrast to expectations from the theory of Galactic chemical evolution.

Our presolar SiC results testify to the utility of the particle mapping system described here. We have also used the system to identify rare presolar Al_2O_3, TiO_2, and $MgAl_2O_4$ grains in meteorite acid residues by measuring $^{17}O/^{16}O$ and $^{18}O/^{16}O$ ratios (Nittler and Alexander, 1999; Nittler et al., 2001) and to search for presolar silicates. Details of these studies will be provided elsewhere.

REFERENCES

Aléon J., Chaussidon M., Marty B., Schutz L., and Jaenicke R. (2002) Oxygen isotopes in single micrometer-sized quartz grains: Tracing the source of Saharan dust over long distance atmospheric transport. *Geochim. Cosmochim. Acta* **66,** 3351–3365.

Alexander C. M. O'D. (1993) Presolar SiC in chondrites: How variable and how many sources? *Geochim. Cosmochim. Acta* **57,** 2869–2888.

Alexander C. M. O'D. and Nittler L. R. (1999) The Galactic chemical evolution of Si, Ti and O isotopes. *Astrophys. J.* **519,** 222–235.

Alexander C. M. O'D., Swan P., and Walker R. M. (1990) *In situ* measurement of interstellar silicon carbide in two CM chondrite meteorites. *Nature* **348,** 715–717.

Amari S., Gao X., Nittler L. R., Zinner E., José J., Hernanz M., and Lewis R. S. (2001a) Presolar grains from novae. *Astrophys. J.* **551,** 1065–1072.

Amari S., Hoppe P., Zinner E., and Lewis R. S. (1992) Interstellar SiC with unusual isotopic compositions: Grains from a supernova? *Astrophys. J.* **394,** L43–L46.

Amari S., Lewis R. S., and Anders E. (1994) Interstellar grains in meteorites. I. Isolation of SiC, graphite, and diamond: Size distributions of SiC and graphite. *Geochim. Cosmochim. Acta* **58,** 459–470.

Amari S., Nittler L. R., Zinner E., Gallino R., Lugaro M., and Lewis R. S. (2001b) Presolar SiC grains of type Y. Origin from low metallicity asymptotic giant branch stars. *Astrophys. J.* **546,** 248–266.

Amari S., Nittler L. R., Zinner E., Lodders K., and Lewis R. S. (2001c) Presolar SiC grains of type A, and B. Their isotopic compositions and stellar origins. *Astrophys. J.* **559,** 463–483.

Amari S., Zinner E., and Lewis R. S. (2000) Isotopic compositions of different presolar SiC size fractions from the Murchison meteorite. *Meteorit. Planet. Sci.* **35,** 997–1014.

Anders E. and Zinner E. (1993) Interstellar grains in primitive meteorites: Diamond, silicon carbide, and graphite. *Meteoritics* **28,** 490–514.

Barnes I. L., Moore L. J., Machlan L. A., Murphy T. J., and Shields W. R. (1975) Absolute isotopic abundance ratios and atomic weight of a reference sample of silicon. *J. Res. Nat. Bur. Stand.* **79A,** 727–735.

Bernatowicz T., Swan P., Messenger S., Walker R. and Amari S. (2000). Comparative morphology of pristine and chemical-dissolution presolar SiC from Murchison. *Lunar Planet. Sci. Conf.* **XXXI,** Abstract #1238 (CD-ROM).

Besmehn A, Hoppe P (2003). A nanoSIMS study of Si- and Ca-Ti-isotopic compositions of presolar silicon carbide grains from supernovae. *Geochim. Cosmochim. Acta* **67**(24), 4693–4703.

Boothroyd A. I. and Sackmann I.-J. (1999) The CNO-isotopes: Deep circulation in red giants and first and second dredge-up. *Astrophys. J.* **510,** 232–250.

Boothroyd A. I., Sackmann I.-J., and Wasserburg G. J. (1995) Hot bottom burning in asymptotic giant branch stars and its effect on oxygen isotopic abundances. *Astrophys. J.* **442,** L21–L24.

Busso M., Gallino R., and Wasserburg G. J. (1999) Nucleosynthesis in asymptotic giant branch stars: Relevance for galactic enrichment and solar system formation. *Annu. Rev. Astron. Astrophys.* **37,** 239–309.

Cameron A. G. W. and Fowler W. A. (1971) Li and the s-process in red-giant stars. *Astrophys. J.* **164,** 111–114.

Charbonnel C. (1995) A consistent explanation for $^{12}C/^{13}C$, ^7Li, and ^3He anomalies in red giant stars. *Astrophys. J.* **453,** L41–L44.

Clayton D. D. (1988) Isotopic anomalies: Chemical memory of galactic evolution. *Astrophys. J.* **334,** 191–195.

Cody G. D., Alexander C. M. O'D., and Tera F. (2002) Solid state (^1H and ^{13}C) NMR spectroscopy of the insoluble organic residue in the Murchison meteorite: A self-consistent quantitative analysis. *Geochim. Cosmochim. Acta* **66,** 1851–1865.

Denissenkov P. A. and Weiss A. (1996) Deep diffusive mixing in globular-cluster red giants. *Astron. Astrophys.* **308,** 773–784.

Frost C. A., Cannon R. C., Lattanzio J. C., Wood P. R., and Forestini M. (1998) The brightest carbon stars. *Astron. Astrophys.* **332,** L17–L20.

Gao X. and Nittler L. R. (1997) ^{30}Si-enriched presolar SiC in Acfer 094 (abstract). *Lunar Planet. Sci. Conf.* **28,** 393–394.

Gehrz R. D., Truran J. W., Williams R. E., and Starrfield S. (1998) Nucleosynthesis in classical novae and its contribution to the interstellar medium. *Publications of the Astronomical Society of the Pacific* **110,** 3–26.

Hoppe P., Amari S., Zinner E., Ireland T., and Lewis R. S. (1994) Carbon, nitrogen, magnesium, silicon, and titanium isotopic compositions of single interstellar silicon carbide grains from the Murchison carbonaceous chondrite. *Astrophys. J.* **430,** 870–890.

Hoppe P., Annen P., Strebel R., Eberhardt P., Gallino R., Lugaro M., Amari S., and Lewis R. S. (1997) Meteoritic silicon carbide grains with unusual Si-isotopic compositions: Evidence for an origin in low-mass, low-metallicity asymptotic giant branch stars. *Astrophys. J.* **487,** L101–104.

Hoppe P, Ott U (1997) Mainstream silicon carbide grains from meteorites. In *Astrophysical Implications of the Laboratory Study of Presolar Materials* (eds. T. J. Bernatowicz and E. K. Zinner), pp. 27–58. AIP Conference Proceedings 402.

Hoppe P., Strebel R., Eberhardt P., Amari S., and Lewis R. S. (1996a) Small SiC grains and a nitride grain of circumstellar origin from the Murchison meteorite: Implications for stellar evolution and nucleosynthesis. *Geochim. Cosmochim. Acta* **60,** 883–907.

Hoppe P., Strebel R., Eberhardt P., Amari S., and Lewis R. S. (1996b) Type II supernova matter in a silicon carbide grain from the Murchison meteorite. *Science* **272,** 1314–1316.

Hoppe P., Strebel R., Eberhardt P., Amari S., and Lewis R. S. (2000) Isotopic properties of silicon carbide X grains from the Murchison meteorite in the size range 0.5–1.5 μm. *Meteorit. Planet. Sci.* **35,** 1157–1176.

Huss G. R., Hutcheon I. D., and Wasserburg G. J. (1997) Isotopic systematics of presolar silicon carbide from the Orgueil (CI) chondrite: Implications for solar-system formation and stellar nucleosynthesis. *Geochim. Cosmochim. Acta* **61** (*23*), 5117–5148.

Huss G. R. and Lewis R. S. (1995) Presolar diamond, SiC, and graphite in primitive chondrites: Abundances as a function of meteorite class and petrologic type. *Geochim. Cosmochim. Acta* **59,** 115–160.

Iben I., Jr. and Renzini A. (1983) Asymptotic giant branch evolution and beyond. *Ann. Rev. Astron. Astrophys.* **21,** 271–342.

José J. and Hernanz M. (1998) Nucleosynthesis in classical novae: CO versus ONe white dwarfs. *Astrophys. J.* **494,** 680–690.

Lugaro M., Davis A. M., Gallino R., Pellin M. J., Straniero O. and Käppeler F. (2003). Isotopic compositions of strontium, zirconium, molybdenum and barium in single presolar SiC grains and asymptotic giant branch stars. *Astrophys. J.* **593,** 486–508.

Lugaro M., Zinner E., Gallino R., and Amari S. (1999) Si isotopic ratios in mainstream presolar SiC grains revisited. *Astrophys. J.* **527,** 369–394.

Nicolussi G. K., Davis A. M., Pellin M. J., Lewis R. S., Clayton R. N., and Amari S. (1997) *s*-Process zirconium in presolar silicon carbide grains. *Science* **277,** 1281–1283.

Nicolussi G. K., Pellin M. J., Lewis R. S., Davis A. M., Amari S., and Clayton R. N. (1998a) Molybdenum isotopic composition of individual presolar silicon carbide grains from the Murchison meteorite. *Geochim. Cosmochim. Acta* **62,** 1093–1104.

Nicolussi G. K., Pellin M. J., Lewis R. S., Davis A. M., Clayton R. N., and Amari S. (1998b) Strontium isotopic composition in individual circumstellar silicon carbide grains: A record of *s*-process nucleosynthesis. *Phys. Rev. Lett.* **81,** 3583–3586.

Nittler L., Alexander C. M. O'D., Gao X., Walker R. M., and Zinner E. (1994) Interstellar oxide grains from the Tieschitz ordinary chondrite. *Nature* **370,** 443–446.

Nittler L., Alexander C. M. O'D., Gao X., Walker R. M., and Zinner E. (1997) Stellar sapphires: The properties and origins of presolar Al_2O_3 in meteorites. *Astrophys. J.* **483,** 475–495.

Nittler L. R (1996) Quantitative isotopic ratio ion imaging and its application to studies of preserved stardust in meteorites. Ph.D., Washington University.

Nittler L. R (2002). Meteoritic stardust and the clumpiness of galactic chemical evolution. *Lunar Planet. Sci. Conf.* **XXXIII,** Abstract #1650 (CD-ROM).

Nittler L. R. (2003) Presolar stardust in meteorites: Recent advances and scientific frontiers. *Earth Planet. Sci. Lett.* **209,** 259–273.

Nittler L. R. and Alexander C. M. O'D. (1999) Automatic identification of presolar Al- and Ti-rich oxide grains from ordinary chondrites. *Lunar Planet. Sci. Conf.* **XXX,** Abstract #2041 (CD-ROM).

Nittler L. R., Alexander C. M. O'D., and Tera F. (2001) Presolar oxide grains from Tieschitz and Murchison (abstract). *Meteorit. Planet. Sci.* **36** (*Suppl.*)**,** A149.

Nittler L. R., Amari S., Zinner E., Woosley S. E., and Lewis R. S. (1996) Extinct ^{44}Ti in presolar graphite and SiC: Proof of a supernova origin. *Astrophys. J.* **462,** L31–L34.

Nittler L. R., Hoppe P., Alexander C. M. O'D., Amari S., Eberhardt P., Gao X., Lewis R. S., Strebel R., Walker R. M., and Zinner E. (1995) Silicon nitride from supernovae. *Astrophys. J.* **453,** L25–L28.

Nollett K. M., Busso M., and Wasserburg G. J. (2003) Cool bottom processes on the thermally-pulsing AGB and the isotopic composition of circumstellar dust grains. *Astrophys. J.* **582,** 1036–1058.

Savina M. R., Davis A. M., Tripa C. E., Pellin M. J., Clayton R. N., Lewis R. S., Amari S., Gallino R. and Lugaro M. (2003). Barium isotopes in individual presolar silicon carbide grains from the Murchison meteorite. *Geochim. Cosmochim. Acta* **67,** 3201–3214.

Simons D. S., Gillen G., Zeissler C. J., Fleming R. H., and McNitt P. J. (1998) Automated SIMS for determining isotopic distributions in particle populations. In *SIMS XI* (eds. G. Gillen, R. Lareau, J. Bennett, and F. Stevie), pp. 59–62. John Wiley and Sons.

Smith V. V. and Lambert D. L. (1990) The chemical composition of red giants. III. Further CNO isotopic and s-process abundances in thermally pulsing asymptotic giant branch stars. *Astrophys. J. Supp.* **72,** 387–416.

Speck A. K., Barlow M. J., and Skinner C. J. (1997) The nature of silicon carbide: Astronomical observations versus meteoritic evidence. *Meteorit. Planet. Sci.* **32,** 703–712.

Straniero O., Chieffi A., Limongi M., Busso M., Gallino R., and Arlandini C. (1997) Evolution and nucleosynthesis in low-mass asymptotic giant branch stars. I. Formation of population I carbon stars. *Astrophys. J.* **478,** 332.

Stroud R. M., O'Grady M., Nittler L. R. and Alexander C. M. O'D. (2002). Transmission electron microscopy of an *in situ* presolar silicon carbide grain. *Lunar Planet. Sci. Conf.* **XXXIII,** Abstract #1785 (CD-ROM).

Tamborini G. and Betti M. (2000) Characterization of radioactive particles by SIMS. *Mikrochimica Acta* **132,** 411–417.

Timmes F. X. and Clayton D. D. (1996) Galactic evolution of silicon isotopes: Application to presolar SiC grains from meteorites. *Astrophys. J.* **472,** 723–741.

Travaglio C., Gallino R., Amari S., Zinner E., Woosley S., and Lewis R. S. (1999) Low-density graphite grains and mixing in type II supernovae. *Astrophys. J.* **510,** 325–354.

Virag A., Wopenka B., Amari S., Zinner E. K., Anders E., and Lewis R. S. (1992) Isotopic, optical and trace element properties of large single SiC grains from the Murchison meteorite. *Geochim. Cosmochim. Acta* **56,** 1715–1733.

Wasserburg G. J., Boothroyd A. I., and Sackmann I.-J. (1995) Deep circulation in red giant stars: A solution to the carbon and oxygen isotope puzzles? *Astrophys. J.* **447,** L37–L40.

Whittet D. C. B. (2002) Dust in the Galactic Environment. 2nd ed. Institute of Physics Publishing, Bristol and Philadelphia.

Zinner E (1989) Isotopic measurements with the ion microprobe. In *New Frontiers in Stable Isotope Research: Laser Probes, Ion Probes and Small-Sample Analysis* (eds. W. C. Shanks III and R. E. Criss), pp. 145–162. USGS Bulletin 1890.

Zinner E. (1998) Stellar nucleosynthesis and the isotopic composition of presolar grains from primitive meteorites. *Annu. Rev. Earth Planet. Sci.* **26,** 147–188.

Zinner E., Tang M., and Anders E. (1989) Interstellar SiC in the Murchison and Murray meteorites: Isotopic composition of Ne, Xe, Si, C, and N. *Geochim. Cosmochim. Acta* **53,** 3273–3290.